Research Square

Preprints are preliminary reports that have not undergone peer review.
They should not be considered conclusive, used to inform clinical practice,
or referenced by the media as validated information.

A locked 468-gene detoxification panel in Alzheimer's disease brain, liver, and blood: 141 high-confidence cerebral associations including lower CYP46A1 transcript abundance, and a 12-sample hepatic CYP7A1 signal

Mark E. McCaulley

mark@siriusneuroscience.com

Sirius Neuroscience, LLC https://orcid.org/0000-0003-2059-622X

Research Article

Keywords: detoxification, redox, cytochrome P450, sterol elimination, oxysterol, bile acid, CYP46A1, CYP7A1, Alzheimer's disease, transcriptomic meta-analysis

Posted Date: September 15th, 2026

DOI: https://doi.org/10.21203/rs.3.rs-10999456/v1

License: This work is licensed under a Creative Commons Attribution 4.0 International License.
Read Full License

Additional Declarations: The authors declare potential competing interests as follows: The author is the sole inventor on a filed patent application relating to panel-based research scoring methods that use the locked 468-gene list reported here. The application did not determine gene membership, the high-confidence rule, or the reported results, and the constructs described here are stated to be unvalidated. Academic reuse of the deposited panel and code does not require a license from the author. The author declares no other competing interests.

Abstract

Detoxification gene expression in Alzheimer's disease (AD) has been examined almost exclusively in brain. Whether the same genes move in the same direction in peripheral organs is unknown. Here a single locked, pre-specified 468-gene redox, metal-homeostasis, xenobiotic-metabolism, and barrier panel is applied to three compartments under one analytic rule.

In brain, inverse-variance random-effects meta-analysis (DerSimonian–Laird) across six independent postmortem adult-brain GEO cohorts (GSE33000, GSE132903, GSE173955, GSE159699, GSE5281, GSE48350) yielded 458 analyzable panel genes, 167 at Benjamini–Hochberg FDR < 0.05, and 141 high-confidence genes (FDR < 0.05, measured in at least three cohorts, direction-concordant in at least 70% of cohorts, and nominally significant in at least two cohorts). High-confidence down-regulation included CYP26A1, TXN, GSS, ATP1A3, and SLC30A3; high-confidence up-regulation included metallothionein family members (MT1F, MT1E, MT2A), PPARA, and FOXO1. Heterogeneity was often high (median I^2 among high-confidence genes 79.3%).

Within that high-confidence set, three genes of the cholesterol-to-oxysterol-to-bile-acid pathway were informative in all six cohorts: cholesterol 24-hydroxylase CYP46A1 was down-regulated (−0.10; FDR = 0.035), while sterol 27-hydroxylase CYP27A1 (+0.17; FDR = 0.048) and CYP39A1 (+0.14; FDR = 0.018) were up-regulated. Because brain cholesterol is separated from the circulating pool by the blood-brain barrier and must be converted to an oxysterol to be exported at all, this is a direction-concordant transcript shift in the principal cerebral cholesterol-disposal route, not a measurement of enzyme activity or sterol flux.

In liver, primary RNA sequencing of commercially bio-banked human hepatic tissue (7 AD, 5 control; 12 samples) is hypothesis-generating and showed a signature unrelated to the central one. In the primary all-case against all-control contrast, five panel genes reached significance: CYP7A1 up-regulated ($\log_2$ fold-change +5.65; $Q = 1.5 \times 10^{-6}$), NOTUM (+4.30) and CYP4F22 (+3.00) up, and CYP17A1 (−4.47) and CYP2S1 (−1.77) down. Hepatic change is therefore concentrated on the bile-acid and steroidogenic axes rather than being a uniform induction or loss of xenobiotic-metabolizing capacity. CYP26B1 was down-regulated in every subgroup contrast involving male Alzheimer's donors and none involving female donors (−2.54; $Q = 1.5 \times 10^{-6}$); other cytochromes reaching significance did so only against the two male controls and are reported as exploratory.

In a supporting peripheral-blood contrast (GSE63060, AddNeuroMed, n = 329), the panel signal was dominated instead by mitochondrial transcripts (NDUFA1 −1.10, NDUFS5 −0.92, COX7C −0.79, MRPL51 −0.57), with a lower-magnitude detoxification component.

Brain, liver, and blood were independent donor collections, not paired samples from the same individuals. The three compartments therefore do not move together. Central detoxification transcripts show metallothionein induction with reduced glutathione-synthesis and thioredoxin abundance, while the small hepatic cohort is dominated by CYP7A1 rather than a uniform xenobiotic-metabolizing shift. These

are transcript-abundance observations and do not establish enzyme activity, flux, or causal direction. The hepatic cohort is small (n = 12) and all hepatic and sex-stratified findings are hypothesis-generating. Published AD-associated variants are tabulated alongside expression rather than merged with it; the Genetic Vulnerability Index, Detoxification Dysregulation Index, and Integrated Detoxification Risk Score are uncalibrated research constructs and are not diagnostic, prognostic, or treatment-selection tools.

ONE-SENTENCE SUMMARY

A locked 468-gene detoxification panel yields 141 high-confidence associations in Alzheimer's disease brain — including lower cholesterol 24-hydroxylase (CYP46A1) with higher CYP27A1 and CYP39A1 — while a separate 12-sample hepatic RNA-sequencing cohort shows a large but hypothesis-generating CYP7A1 increase; the three compartments do not move together, and GVI, DDI, and IDRS remain unvalidated research constructs.

INTRODUCTION

Alzheimer's disease (AD) remains the leading cause of dementia worldwide, affecting an estimated 55 million individuals globally with projections reaching 139 million by 2050 (1–3). Despite decades of research and substantial investment, the initiating molecular events remain incompletely understood, and disease-modifying treatments have proven elusive (2).

This analysis extends a peer-reviewed two-phase study of detoxification gene expression in AD (4). That work applied a 203-gene detoxification panel in two phases. Phase 1 analyzed seven publicly archived RNA-sequencing series (GSE104704, GSE159699, GSE153873, GSE173955, GSE211993, GSE227221, GSE190125). Phase 2 was primary RNA sequencing of commercially bio-banked human liver tissue (7 AD, 5 control), performed by LC Sciences. Across both phases, 162 detoxification genes showed significant differential expression — 154 in the archived series and 69 in the liver tissue, with 61 shared — and the study reported metallothionein up-regulation alongside reduced glutathione-synthesis transcripts.

The present analysis carries that work forward in four ways. First, the panel is expanded from 203 genes to a locked, functional-family-enumerated 468-gene panel that was frozen before these analyses and is deposited unchanged. Second, the primary inference is replaced: instead of per-dataset differential expression, a six-cohort inverse-variance random-effects meta-analysis is performed under a pre-specified high-confidence rule. Third, published AD-associated variants are tabulated alongside expression rather than merged into a score. Fourth, and most importantly, the same locked panel is applied to three compartments — brain, liver, and peripheral blood — so that directional concordance between the central nervous system and the periphery can be assessed rather than assumed.

Six of the seven archived series analyzed in the earlier work reappear here: GSE159699 and GSE173955 as primary meta-analysis cohorts, and GSE211993, GSE227221, GSE190125, and GSE153873 as supporting contrasts. GSE104704 was screened and not admitted to the primary set (see Materials and

Methods). The earlier directional findings for MT2A and GSS both reproduce here under the expanded panel and the stricter rule, providing internal replication across two panel versions, two analytic pipelines, and an expanded cohort set.

The motivating question is compartmental. Detoxification is not a brain-specific process. The liver is the principal site of xenobiotic metabolism in the body, and hepatic cytochrome P450 capacity determines systemic clearance of the compounds that reach the central nervous system. If detoxification-related transcripts are altered in AD brain, the natural next question is whether the periphery shows the same change, the opposite change, or none. That question has not previously been asked with a single pre-specified panel applied identically across compartments, and it is the principal contribution of this analysis.

The rationale for tabulating genetics alongside expression is separate and more limited. Expression levels reflect current pathway activity, whereas genetic variants determine the baseline capacity of the encoded enzyme. An individual with normal GSTM1 expression but carrying the GSTM1 null genotype produces no functional enzyme regardless of expression level (5–7). Both layers can be tabulated; they are not combined here into a validated risk tool. An additive research index (IDRS) is shown only as a worked numerical example. It is not offered as a population risk tool or as a basis for personalized therapy, and prospective validation against clinical outcomes has not been performed.

RESULTS

Compartment 1 — Brain: six-cohort adult-brain meta-analysis

Primary inference is the six-cohort adult-brain random-effects meta-analysis (GSE33000, GSE132903, GSE5281, GSE48350 microarray, Braak stage IV or greater versus code-C controls, 61 versus 140; GSE173955 and GSE159699 RNA-seq). Two of the six cohorts are RNA-seq and four are microarray; they are combined only at the per-gene effect-size level under the locked high-confidence rule, never by merging raw expression.

Of 468 panel genes, 458 were meta-analyzable. One hundred sixty-seven reached Benjamini–Hochberg FDR < 0.05, of which 141 met the locked high-confidence rule. High-confidence down-regulated transcripts included CYP26A1, TXN, GSS, ATP1A3, and SLC30A3. High-confidence up-regulated transcripts included metallothionein family members (MT1F, MT1E, MT2A), PPARA, and FOXO1. Median I^2 among high-confidence genes was 79.3%, so pooled brain effects should be read with that heterogeneity in view.

The dominant brain pattern is therefore metal-handling induction set against reduced glutathione-synthesis and thioredoxin transcript abundance. These are transcript observations. They do not establish glutathione flux, enzyme activity, or GSH/GSSG status.

A second brain result sits inside the high-confidence set and has not previously been drawn out of it. Three genes of the cholesterol-to-oxysterol-to-bile-acid pathway meet the locked rule, each informative in all six cohorts. CYP46A1, cholesterol 24-hydroxylase, is down (pooled $\log_2$ fold-change −0.10; FDR = 0.035). CYP27A1, sterol 27-hydroxylase, is up (+0.17; FDR = 0.048). CYP39A1, which 7α-hydroxylates the CYP46A1 product, is up (+0.14; FDR = 0.018). CYP46A1 is the enzyme by which the brain converts cholesterol to 24S-hydroxycholesterol for export across the blood-brain barrier, and it carries the quantitatively dominant route of cerebral cholesterol turnover. These pooled effects are small, as most in this meta-analysis are, but they are direction-concordant across all six cohorts: lower transcript abundance for the principal cholesterol-export enzyme alongside higher abundance for the alternative oxysterol route. They are transcript shifts, not measurements of enzyme capacity or sterol flux.

For contrast, only one inflammation-associated panel gene meets the high-confidence rule: NFKB1 (+0.32; FDR = 0.031, four cohorts). The panel contains no cytokine, inflammasome, or microglial-receptor genes, so this is a statement about what was measured rather than about the role of inflammation in the disease.

Because two of the six cohorts are RNA-sequencing and four are microarray, the natural question is whether the pooled result is carried by the microarray cohorts. The per-gene cohort count answers it directly. Of the 141 high-confidence genes, 102 (72.3%) were informative in all six cohorts and therefore in both RNA-sequencing cohorts, and a further 10 were informative in five. Since only four microarray cohorts exist, any gene informative in five or more cohorts must draw on at least one RNA-sequencing cohort: 112 of 141 high-confidence genes (79.4%) do so. At most 29 (20.6%) could in principle rest on microarray cohorts alone. The same pattern holds one level up, among the 167 FDR-significant genes (113 at six cohorts, 126 at five or more), and among all 458 analyzable genes (253 and 306 respectively).

Two further checks point the same way and are reported in full in the Supplementary Materials. A scale-free Stouffer combination of per-cohort z-scores, which ignores fold-change magnitude and so cannot be distorted by mixing platform scales, reproduced 98% of the effect-size-pooled calls (108 of 110 overlapping). Per-cohort sign concordance with the pooled direction was 81% to 100%, with the two RNA-sequencing cohorts contributing 103 and 104 significant panel-gene calls against 106 and 99 for the two largest microarray cohorts, so the sequencing cohorts are not passengers in the pool. The high-confidence rule itself requires independent nominal significance in at least two cohorts; among the 141 high-confidence genes the median was four, and 79 (56.0%) were independently significant in four or more.

The microarray cohorts are retained for a positive reason as well as a numerical one. They supply the regional spread that the sequencing arm does not: prefrontal cortex (GSE33000, n = 624), middle temporal gyrus (GSE132903), multiple cortical regions (GSE5281), and hippocampus with cortex (GSE48350). The two sequencing cohorts are themselves non-redundant — GSE173955 is hippocampus from the Japanese Hisayama cohort and GSE159699 is lateral temporal lobe from a United States cohort — but between them they cover two regions and two populations. Restricting the primary analysis

to RNA sequencing would therefore have reduced it to two cohorts of roughly 18 to 30 subjects each across two regions, which is a weaker design than six cohorts across several regions with platform modelled as a heterogeneity term. The sequencing cohorts are also smaller than the largest array cohorts, which is why effects are pooled by inverse-variance weighting rather than by vote counting, and why the high-confidence rule requires independent significance in at least two cohorts rather than deferring to the largest.

Gene	Direction	Pooled log_2FC	95% CI	I^2	FDR
HSPA1A	up	0.66	0.28, 1.04	77%	3.0×10^{-3}
MT1F	up	0.57	0.36, 0.77	77%	1.4×10^{-6}
MT1M	up	0.55	0.29, 0.81	88%	2.5×10^{-4}
MAFF	up	0.54	0.32, 0.76	85%	3.5×10^{-5}
MT1H	up	0.53	0.32, 0.75	84%	1.7×10^{-5}
MT2A	up	0.51	0.27, 0.76	92%	3.9×10^{-4}
SLCO4A1	up	0.44	0.21, 0.67	88%	1.3×10^{-3}
ADH1B	up	0.44	0.16, 0.72	97%	8.5×10^{-3}
MT1A	up	0.43	0.21, 0.65	69%	8.5×10^{-4}
MT1E	up	0.42	0.26, 0.59	80%	7.5×10^{-6}
FOXO4	up	0.41	0.24, 0.58	91%	2.1×10^{-5}
MT1G	up	0.40	0.23, 0.57	73%	5.9×10^{-5}
TXNIP	up	0.38	0.16, 0.61	80%	4.2×10^{-3}
VCAM1	up	0.38	0.15, 0.60	73%	4.5×10^{-3}
AKR1C3	up	0.35	0.22, 0.48	64%	5.2×10^{-6}
IRF7	up	0.35	0.11, 0.60	87%	1.8×10^{-2}
MT1X	up	0.35	0.10, 0.59	89%	1.8×10^{-2}
FMO2	up	0.33	0.13, 0.53	90%	6.1×10^{-3}
NFKB1	up	0.32	0.07, 0.56	94%	3.1×10^{-2}
SLC47A2	up	0.31	0.19, 0.43	55%	1.8×10^{-5}
STEAP4	up	0.31	0.15, 0.48	57%	1.2×10^{-3}
DNAJB1	up	0.31	0.06, 0.57	68%	4.3×10^{-2}
FOXO1	up	0.30	0.19, 0.42	83%	1.6×10^{-6}
ABCA1	up	0.29	0.18, 0.40	67%	6.3×10^{-6}
CGN	up	0.29	0.13, 0.45	89%	1.9×10^{-3}
TJP2	up	0.29	0.13, 0.45	81%	2.0×10^{-3}
NXN	up	0.25	0.13, 0.38	83%	6.7×10^{-4}
RXRA	up	0.24	0.11, 0.37	85%	1.1×10^{-3}

Gene	Direction	Pooled log_2FC	95% CI	I^2	FDR
SP1	up	0.24	0.07, 0.40	86%	1.9×10^{-2}
PECAM1	up	0.23	0.09, 0.38	76%	8.3×10^{-3}
ALDH1L1	up	0.21	0.12, 0.30	45%	9.2×10^{-5}
CBS	up	0.21	0.09, 0.32	73%	1.9×10^{-3}
SIRT1	up	0.21	0.09, 0.34	88%	4.5×10^{-3}
SLCO2B1	up	0.21	0.08, 0.34	71%	4.8×10^{-3}
GSTM2	up	0.21	0.08, 0.34	75%	7.8×10^{-3}
PPARA	up	0.20	0.14, 0.27	66%	1.0×10^{-7}
TJP1	up	0.20	0.09, 0.31	80%	2.0×10^{-3}
PRDX6	up	0.18	0.10, 0.26	53%	2.1×10^{-4}
HSD17B1	up	0.18	0.07, 0.28	83%	4.0×10^{-3}
CHST12	up	0.18	0.07, 0.30	90%	6.8×10^{-3}
PAPSS2	up	0.18	0.03, 0.33	62%	4.9×10^{-2}
CHST14	up	0.17	0.08, 0.25	81%	9.8×10^{-4}
CYP27A1	up	0.17	0.03, 0.31	75%	4.8×10^{-2}
FMO3	up	0.16	0.05, 0.27	88%	1.2×10^{-2}
CYP4F12	up	0.16	0.04, 0.27	86%	2.7×10^{-2}
SULT1B1	up	0.15	0.03, 0.28	95%	4.8×10^{-2}
SLCO1A2	up	0.14	0.08, 0.21	51%	2.6×10^{-4}
CYP2J2	up	0.14	0.06, 0.23	51%	4.2×10^{-3}
CYP39A1	up	0.14	0.04, 0.24	92%	1.8×10^{-2}
PON3	up	0.14	0.04, 0.24	66%	2.5×10^{-2}
ABCC2	up	0.13	0.04, 0.22	92%	2.0×10^{-2}
SLC22A3	up	0.12	0.05, 0.19	77%	5.1×10^{-3}
SLC22A5	up	0.11	0.05, 0.16	60%	7.7×10^{-4}
MGST2	up	0.11	0.03, 0.19	72%	3.1×10^{-2}
ANPEP	up	0.11	0.02, 0.19	92%	3.6×10^{-2}
FMO5	up	0.10	—	1%	underflow

Gene	Direction	Pooled log_2FC	95% CI	I^2	FDR
CAT	up	0.10	0.04, 0.15	29%	2.4×10^{-3}
SLC40A1	up	0.10	0.03, 0.17	45%	1.6×10^{-2}
MTF1	up	0.09	0.03, 0.14	60%	6.7×10^{-3}
SLC22A1	up	0.09	0.03, 0.15	73%	9.9×10^{-3}
JAM2	up	0.09	0.03, 0.16	35%	1.8×10^{-2}
IKBKE	up	0.08	—	6%	underflow
BACH1	up	0.08	0.03, 0.14	86%	1.3×10^{-2}
ARNT	up	0.08	0.02, 0.14	66%	2.0×10^{-2}
CYP2S1	up	0.07	0.05, 0.09	21%	1.1×10^{-9}
CYP19A1	up	0.07	0.02, 0.11	70%	3.2×10^{-2}
ICAM1	up	0.06	0.01, 0.11	52%	4.0×10^{-2}
RARG	up	0.05	0.01, 0.09	70%	2.3×10^{-2}
FOXO3	up	0.05	0.01, 0.09	33%	2.7×10^{-2}
KEAP1	up	0.04	0.03, 0.06	0%	1.1×10^{-9}
SLC30A6	up	0.04	0.03, 0.05	0%	5.2×10^{-9}
PON1	up	0.04	0.01, 0.08	69%	4.1×10^{-2}
UGT2A1	up	0.03	0.02, 0.04	0%	1.4×10^{-7}
PTGS1	up	0.03	0.01, 0.05	0%	7.6×10^{-4}
GCH1	up	0.03	0.01, 0.05	0%	1.7×10^{-3}
ADH1C	up	0.02	0.02, 0.03	0%	5.5×10^{-7}
SULT4A1	down	-0.69	-1.03, -0.35	94%	4.7×10^{-4}
SLC30A3	down	-0.64	-0.92, -0.37	92%	6.6×10^{-5}
ATP1A3	down	-0.63	-0.88, -0.37	92%	2.1×10^{-5}
ATP1A1	down	-0.51	-0.74, -0.29	93%	9.8×10^{-5}
CYP26B1	down	-0.44	-0.70, -0.18	90%	4.0×10^{-3}
EPHX4	down	-0.44	-0.72, -0.17	70%	6.3×10^{-3}
ATP1B1	down	-0.43	-0.63, -0.23	93%	2.1×10^{-4}
CYP4X1	down	-0.43	-0.64, -0.22	91%	4.2×10^{-4}

Gene	Direction	Pooled log_2FC	95% CI	I^2	FDR
COX5A	down	-0.38	-0.58, -0.18	90%	1.6×10^{-3}
TXN	down	-0.37	-0.50, -0.24	92%	1.2×10^{-6}
GLRX	down	-0.37	-0.58, -0.16	90%	3.5×10^{-3}
CYP26A1	down	-0.31	—	12%	underflow
PSMA1	down	-0.31	-0.53, -0.10	88%	1.6×10^{-2}
GSS	down	-0.30	-0.41, -0.19	91%	2.1×10^{-6}
USP14	down	-0.29	-0.48, -0.10	87%	8.8×10^{-3}
CYCS	down	-0.28	-0.40, -0.16	70%	5.9×10^{-5}
GSTA4	down	-0.28	-0.43, -0.14	89%	6.7×10^{-4}
ACSL4	down	-0.27	-0.42, -0.11	86%	4.2×10^{-3}
SLC30A9	down	-0.26	-0.37, -0.16	77%	7.3×10^{-6}
SOD1	down	-0.26	-0.38, -0.14	91%	2.2×10^{-4}
STS	down	-0.26	-0.47, -0.06	95%	3.3×10^{-2}
GLRX2	down	-0.25	-0.35, -0.14	74%	3.8×10^{-5}
CYP2C8	down	-0.25	-0.37, -0.13	87%	4.7×10^{-4}
GLRX5	down	-0.24	-0.34, -0.14	90%	3.4×10^{-5}
UBB	down	-0.24	-0.35, -0.13	70%	2.1×10^{-4}
HAGH	down	-0.24	-0.39, -0.10	88%	4.7×10^{-3}
NDUFA1	down	-0.24	-0.42, -0.05	90%	3.6×10^{-2}
PRDX5	down	-0.23	-0.34, -0.12	81%	2.8×10^{-4}
GSTO1	down	-0.22	-0.33, -0.12	84%	4.4×10^{-4}
PAPSS1	down	-0.22	-0.34, -0.11	90%	9.8×10^{-4}
NDUFS5	down	-0.22	-0.39, -0.06	88%	2.4×10^{-2}
NDUFS3	down	-0.21	-0.31, -0.11	84%	3.1×10^{-4}
MGST3	down	-0.21	-0.33, -0.09	88%	3.0×10^{-3}
ATOX1	down	-0.21	-0.34, -0.08	92%	5.6×10^{-3}
SLC39A3	down	-0.19	-0.28, -0.11	84%	5.4×10^{-5}
PSMB5	down	-0.19	-0.29, -0.09	69%	1.0×10^{-3}

Gene	Direction	Pooled log_2FC	95% CI	I^2	FDR
ALDH5A1	down	-0.19	-0.31, -0.08	82%	4.2×10^{-3}
ALDH1A1	down	-0.18	-0.26, -0.10	31%	2.1×10^{-4}
GPX4	down	-0.18	-0.29, -0.08	88%	2.4×10^{-3}
AKR1A1	down	-0.18	-0.29, -0.08	88%	4.0×10^{-3}
HMOX2	down	-0.18	-0.29, -0.08	93%	4.2×10^{-3}
SUMO1	down	-0.17	-0.24, -0.10	68%	2.8×10^{-5}
ME1	down	-0.17	-0.28, -0.06	89%	1.2×10^{-2}
BLVRA	down	-0.16	-0.24, -0.08	79%	4.7×10^{-4}
PRDX2	down	-0.16	-0.27, -0.06	84%	1.0×10^{-2}
PSMB4	down	-0.16	-0.28, -0.04	86%	3.0×10^{-2}
PARK7	down	-0.15	-0.22, -0.08	90%	3.5×10^{-4}
PRDX3	down	-0.15	-0.25, -0.06	74%	6.8×10^{-3}
NQO2	down	-0.14	-0.22, -0.06	69%	2.7×10^{-3}
TDO2	down	-0.14	-0.23, -0.05	77%	10.0×10^{-3}
IDH2	down	-0.14	-0.26, -0.03	82%	4.3×10^{-2}
CYP2E1	down	-0.13	-0.18, -0.09	30%	1.9×10^{-6}
ALDH1B1	down	-0.13	-0.20, -0.06	75%	2.1×10^{-3}
PINK1	down	-0.13	-0.21, -0.05	84%	5.0×10^{-3}
CYP51A1	down	-0.12	-0.19, -0.04	51%	1.0×10^{-2}
SLC30A5	down	-0.10	-0.16, -0.04	63%	3.9×10^{-3}
SUOX	down	-0.10	-0.17, -0.04	75%	8.6×10^{-3}
SULT2B1	down	-0.10	-0.16, -0.03	77%	1.2×10^{-2}
CYP46A1	down	-0.10	-0.18, -0.02	61%	3.5×10^{-2}
GSTO2	down	-0.09	-0.14, -0.05	27%	3.6×10^{-4}
GSR	down	-0.08	-0.12, -0.05	43%	1.0×10^{-4}
CYP4Z1	down	-0.08	-0.13, -0.03	78%	3.4×10^{-3}
TPMT	down	-0.08	-0.12, -0.03	48%	8.5×10^{-3}
COX7C	down	-0.06	-0.08, -0.05	1%	1.8×10^{-9}

Gene	Direction	Pooled log_2FC	95% CI	I^2	FDR
CHAC1	down	-0.05	-0.07, -0.03	15%	4.4×10^{-4}

Table 1. The complete set of 141 high-confidence panel genes from the six-cohort adult-brain meta-analysis, ordered by absolute pooled effect. Pooled log_2 fold-change with 95% confidence interval, between-cohort heterogeneity, and Benjamini–Hochberg FDR. The full 167-gene FDR-significant list and the per-gene pooled statistics (k, I^2, P, FDR, cohorts nominally significant, direction concordance) are provided in Table S3 (supplementary workbook), built from the deposited per-gene meta-analysis table. Three genes — FMO5, IKBKE and CYP26A1 — are shown without a confidence interval and with the adjusted P marked as underflow: the deposited per-gene summary records their P and FDR as exactly zero, which is a floating-point underflow rather than a measured quantity, and carries no recoverable standard error. All three meet every other criterion of the high-confidence rule and are retained, but their adjusted P values should be read as unavailable rather than as extreme.

Compartment 2 — Liver: primary hepatic RNA sequencing (n = 12; hypothesis-generating)

Primary RNA sequencing was performed on commercially bio-banked human liver tissue from 7 AD and 5 control donors (12 samples total), sequenced by LC Sciences under an FDR ≤ 0.05 and absolute fold-change ≥ 2 criterion (see Materials and Methods). These samples were previously reported under a 203-gene panel (4); the analysis presented here applies the locked 468-gene panel and addresses a question not examined in that work, namely the directional relationship between hepatic and central detoxification transcripts. No result from the earlier analysis is re-presented as new.

Sample ID	Sex	Age	Diagnosis	PMI (h)	BMI	Autopsy date	Cause of death
091584A(2)	F	96	AD	3.5	20.2	09/23/2019	AD, cerebral edema
091499A(1)	F	79	AD	2	25.5	05/27/2019	AD, cerebral edema
091486A(2)	M	85	AD	4	25.7	05/11/2019	AD, cerebral edema
091485A(3)	M	86	AD	4	25.6	05/11/2019	AD, cerebral edema
091483A(3)	M	85	AD	3.5	25.6	05/04/2019	AD, cerebral edema
091361A(4)	F	65	AD	2.5	26.1	07/03/2018	AD, pneumonia
091260A(4)	F	74	AD	2.5	20.8	09/19/2017	AD, cachexia, bronchopneumonia
091216A(2)	M	90	Control	3	24.8	06/19/2017	Heart failure
091207A(5)	F	81	Control	2.5	25.7	06/09/2017	Postinfarction cardiosclerosis, chronic heart failure
091121A(3)	M	75	Control	2.5	25.9	02/03/2017	Cardiac aneurysm, heart failure
09968A(6)	F	74	Control	4	23.0	04/07/2016	Pulmonary embolism
09630A(2)	F	66	Control	5.5	N/A	07/16/2013	Pulmonary embolism

Table 2. Characteristics of the 12 hepatic tissue donors, from the source study's supplementary metadata (4). All specimens were fresh-frozen liver from Caucasian donors obtained through AMSBIO. Note that autopsy date separates the groups completely: every control was collected before every Alzheimer's case. PMI = post-mortem interval.

In the primary hepatic contrast — all 7 Alzheimer's donors against all 5 controls at gene level — five panel genes met the source study's significance criterion (Table 3). CYP7A1, the rate-limiting enzyme of the classical bile-acid synthesis pathway, was strongly up-regulated ($\log_2$ fold-change +5.65; Q = 1.5×10^{-6}), as were NOTUM (+4.30) and CYP4F22 (+3.00). CYP17A1 (−4.47) and CYP2S1 (−1.77) were down-regulated. The hepatic signature is therefore dominated by a large increase in bile-acid synthase transcript abundance alongside a marked reduction in steroidogenic CYP17A1, and it is not a uniform induction of xenobiotic-metabolizing cytochromes: CYP4F22 rises while CYP2S1 falls.

Additional cytochromes reach significance only in sex-crossed subgroup contrasts with two to four donors per cell, and their attribution requires care. CYP26B1 is down-regulated in every contrast involving Alzheimer's males and in none involving Alzheimer's females (−2.54 against male controls, Q = 1.5×10^{-6}), so it is the one genuinely male-associated hepatic signal. CYP1A1, CYP2A13, CYP3A4, and CYP4F12 behave differently: each reaches significance against the two male controls, in Alzheimer's females as well as Alzheimer's males, which locates the contrast in the comparator group rather than in

the sex of the cases. CYP2D6 reaches significance only in Alzheimer's females against female controls (+3.72, transcript level). None of these supports a claim about xenobiotic-metabolizing capacity in Alzheimer's liver as such.

This matters because several of the same or related CYP transcripts move in the opposite direction centrally. In the CNS compartment, CYP1B1 was the dominant up-regulated CYP across multiple AD-relevant systems (PSEN1 A79V iPSC adjusted P approximately 1×10^{-194}; PSEN1 L150P iPSC adjusted P approximately 2.5×10^{-12}; all microglia timepoints; Trisomy 21 blood adjusted P approximately 10^{-13}), and CYP26A1 was high-confidence down-regulated in the six-cohort brain meta-analysis. Across the per-dataset supporting brain contrasts, by contrast, CYP26 involvement is partial: CYP26B1 is down-regulated in GSE173955 hippocampus ($\log_2$ fold-change approximately −1.34), while CYP26A1 and CYP26C1 do not reach concordant directional change across those individual comparisons. The high-confidence CYP26A1 call rests on the pooled six-cohort estimate, not on any single dataset.

The hepatic cohort comprises 12 samples. Every hepatic observation in this section is hypothesis-generating, is reported without a claim of generalizability, and requires replication in an adequately powered independent liver series.

Gene	Role	log_2FC	Q	Contrast
Primary contrast — all 7 AD vs all 5 control, gene level				
CYP7A1	Cholesterol 7α-hydroxylase; rate-limiting step of bile-acid synthesis	+5.65	1.5×10^{-6}	AD vs control
NOTUM	Palmitoleoyl-protein carboxylesterase; Wnt modulation	+4.30	1.2×10^{-3}	AD vs control
CYP4F22	Fatty-acid ω-hydroxylation; epidermal barrier lipids	+3.00	2.8×10^{-2}	AD vs control
CYP2S1	Xenobiotic and eicosanoid metabolism	−1.77	3.0×10^{-2}	AD vs control
CYP17A1	Steroid 17α-hydroxylase / 17,20-lyase; steroidogenesis	−4.47	4.5×10^{-2}	AD vs control
Exploratory subgroup contrasts — 2 to 4 donors per cell				
CYP26B1	Retinoic-acid catabolism	−2.54	1.5×10^{-6}	AD male vs control male; also −2.78 vs all controls and −2.92 vs control female. Absent from all female-AD contrasts.
CYP1A1	Xenobiotic metabolism; AhR-responsive	+2.56	3.4×10^{-2}	AD male vs control male; also +4.30 ($Q = 5.5 \times 10^{-5}$) AD female vs control male
CYP3A4	Xenobiotic metabolism; most abundant hepatic CYP	+5.30	3.9×10^{-4}	AD male vs control male, transcript level; also +3.79 AD female vs control male
CYP4F12	Fatty-acid and xenobiotic ω-hydroxylation	+1.91	8.1×10^{-4}	AD male vs control male
CYP2D6	Xenobiotic metabolism (debrisoquine 4-hydroxylase)	+3.72	1.1×10^{-2}	AD female vs control female, transcript level. Not significant in the primary contrast.
CYP2A13	Xenobiotic metabolism	+11.34	3.6×10^{-4}	AD male vs control male; also +10.45 AD female vs control male. Magnitude indicates near-absent expression in the comparator.

Table 3. Panel genes reaching significance in Alzheimer's disease liver, from the source study's supplementary differential-expression tables (4). Significance criterion FDR ≤ 0.05 with absolute fold change ≥ 2; Q is the false-discovery-rate-adjusted value. The upper block is the primary contrast — all 7 Alzheimer's donors against all 5 controls at gene level — and is the defensible hepatic result. The lower block reports sex-crossed subgroup contrasts with two to four donors per cell; these are exploratory, and the comparator group is named for each because several of them are defined against the two male controls rather than by the sex of the Alzheimer's donors. Absolute $\log_2$ fold-changes above about 10 indicate near-absent expression in one group rather than a graded difference and should not be read as effect sizes.

Exploratory liver sex-stratified contrasts (not a primary compartment)

A sex-stratified examination of the hepatic data separates one signal from several that look similar but are not. CYP26B1 down-regulation is present in all three contrasts involving male Alzheimer's donors — against all controls (−2.78), against female controls (−2.92), and against male controls (−2.54, Q = 1.5×10^{-6}) — and in none of the contrasts involving female Alzheimer's donors. That pattern is consistent with a male-associated hepatic effect.

The other cytochromes previously grouped with it do not behave that way. CYP1A1, CYP2A13, CYP3A4, and CYP4F12 each reach significance specifically against the two male controls, and do so for female Alzheimer's donors as well as male ones. The common term in those comparisons is the comparator group, not the sex of the cases, so the more parsimonious reading is low expression in two control livers rather than induction in male Alzheimer's livers. An earlier description of these genes as a male-predominant compensatory clearance signature is not supported by the subgroup structure and is not made here.

The cell sizes make this an observation rather than a finding: four female and three male Alzheimer's donors, three female and two male controls. Any contrast against male controls rests on two livers. A sex-differing hepatic clearance pattern would, if reproduced in adequately powered cohorts, be a candidate peripheral correlate of the known female excess in late-life Alzheimer's incidence. Longevity, menopause-related estrogen change, and the APOE by sex interaction remain the established explanations for that excess, and nothing in these 12 samples displaces them.

An exploratory sex-stratified analysis of GSE173955 hippocampus suggested a higher detoxification signal in female than male AD samples. Precise recomputation on the locked DDI definition awaits a sex-stratified differential-expression export, so this observation is reported as hypothesis-generating only.

Compartment 3 — Peripheral blood (supporting contrast; not part of the six-cohort brain meta-analysis)

The peripheral blood dataset GSE63060 (AddNeuroMed consortium, n = 329) (32) was analyzed as a supporting contrast, not as a second primary inference. Its signature was dominated not by detoxification transcripts but by mitochondrial ones: NDUFA1 (−1.10, Complex I), NDUFS5 (−0.92, Complex I), COX7C (−0.79, Complex IV), and MRPL51 (−0.57, mitochondrial ribosome). Antioxidant

transcripts were also lower: TXN (−0.71), SOD1 (−0.41), and PRDX1 (−0.33). All values are $\log_2$ fold-change at Benjamini–Hochberg adjusted $P < 0.05$. The per-dataset DDI for this series is given in Table S1.

This peripheral profile differs from both the brain and hepatic patterns, consistent with tissue-specific pathway utilization in which circulating cells depend more heavily on mitochondrial function while neurons depend predominantly on glutathione-based handling (33). The peripheral detoxification signal is expected to be lower in magnitude than a tissue signal and is reported as such. Whether a blood-based DDI carries prospectively useful information, as opposed to reflecting the central signal only weakly, is untested, and it is the central open question for any deployable expression component of the IDRS.

Cross-compartment discordance

Taken together, the three compartments do not move as one system. Brain shows metallothionein induction with reduced glutathione-synthesis and thioredoxin transcripts. Liver shows a bile-acid and steroidogenic signature — CYP7A1 sharply up, CYP17A1 down — with no coherent direction among xenobiotic-metabolizing cytochromes, CYP4F22 rising while CYP2S1 falls. Blood shows a predominantly mitochondrial profile with a smaller detoxification component.

The relevant comparison is not that hepatic cytochromes move opposite to central ones, which the subgroup structure does not support, but that the two compartments engage different parts of the panel altogether. A model in which detoxification capacity fails uniformly in Alzheimer's disease predicts concordant change in the same gene families across compartments. That is not what these data show. The central signal falls on metal handling and glutathione and thioredoxin synthesis; the hepatic signal falls on bile-acid synthesis and steroidogenesis; and the genes carrying each signal barely overlap.

Three interpretations remain open and are not distinguished by these data. The hepatic change may be a compensatory response to increased systemic burden; it may be an unrelated consequence of the metabolic and nutritional changes that accompany advanced dementia; or it may reflect selection and comorbidity in a small bio-banked series. Discriminating among these requires larger hepatic cohorts with clinical annotation, and ideally protein and activity measurement rather than transcript abundance alone.

What the data do support is narrower and worth stating plainly: detoxification-related transcript change in AD is compartment-specific, and inferences drawn from brain tissue alone should not be generalized to the organism.

Descriptive categories of transcript change

Mutation-specific and tissue-specific patterns can be grouped descriptively by transcript direction — lower, higher, or unchanged — together with a fourth grouping that annotates a direction rather than constituting one of its own (Fig. 1). These labels are interpretive, not treatment assignments:

Lower abundance: core transcripts are down in the stated contrast (examples: GSS and GCLC in some AD tissue contrasts). Function, flux, and treatment response are not measured.

Higher abundance that may be compensatory: examples include metallothionein induction in some sporadic AD tissue contrasts (23, 24). Direction of change does not prove adaptation or a supplementation indication.

Unchanged abundance: a transcript may be unaltered in a contrast even when related pharmacology exists in other systems (example: EPHX2). Absence of differential expression is not an indication to push the node pharmacologically.

Possibly adverse direction: example, higher EPHX2 in L150P, which could increase hydrolysis of epoxyeicosatrienoic acids. That inference is biochemical, not a treatment recommendation.

Transcript direction in a public contrast is not a sufficient basis for choosing an intervention in a patient.

Supporting model contrasts and descriptive DDI values

Table 4 lists supporting and secondary RNA-seq contrasts. Two of those accessions (GSE173955 hippocampus; GSE159699) also contribute to the six-cohort primary meta-analysis. Sex- or age-stratified sub-contrasts are hypothesis-generating only. Per-dataset DDI is defined uniformly across the datasets in this paper as the percentage of measurable panel genes that are both significant at Benjamini–Hochberg adjusted $P < 0.05$, with BH correction computed within the 468-gene panel, and of absolute $\log_2$ fold-change at least 0.5.

An aging-only control provides a specificity check. GSE153873 old versus young, without AD diagnosis, yielded a near-null DDI of 0.9% (4 of 376 measurable panel genes), against 9.4% to 41.2% on the panel basis for disease contrasts. This is consistent with these genes being dysregulated in AD (15) rather than in normal aging.

Dataset	Comparison	DEGs	Meas.	DDI_panel	DDI_meas	Up/Down	TDM
GSE211993	A79V iPSC	63	363	13.5%	17.4%	17/46	78.8
GSE211993	L150P iPSC	148	348	31.6%	42.5%	63/85	234.4
GSE190125	Trisomy 21	52	328	11.1%	15.9%	36/16	39.6
GSE227221	Aβ microglia 4 h	99	289	21.2%	34.3%	64/35	136.9
GSE227221	Aβ microglia 24 h	193	298	41.2%	64.8%	105/88	443.1
GSE227221	Aβ microglia 96 h	146	300	31.2%	48.7%	75/71	298.2
GSE173955	Hippocampus	73	378	15.6%	19.3%	51/22	73.8
GSE159699	Lateral temporal	44	373	9.4%	11.8%	19/25	31.7
GSE153873	AD vs. young	78	376	16.7%	20.7%	23/55	65.5
GSE153873	AD vs. old	5	375	1.1%	1.3%	3/2	6.4

Table 4. Descriptive DDI in supporting RNA-seq contrasts. DDI_panel = differentially expressed genes / 468. DDI_meas = differentially expressed genes / measurable genes. TDM = sum of absolute log_2 fold-change across significant genes. Provisional DDI classification thresholds (Minimal < 7%, Moderate 7–15%, Substantial 15–30%, Severe > 30%) are empirically derived and require prospective validation.

Mutation-specific effects: PSEN1 A79V versus L150P

The two PSEN1 mutations showed broadly overlapping pathway dysregulation at similar aggregate DDI (combined PSEN1 iPSC DDI 39.0% observed; per-genotype A79V 13.5% panel / 17.4% observed; L150P 31.6% / 42.5%; GSE211993), with mutation-specific divergences at individual genes.

In the isogenic A79V contrast, GCLC, GCLM, and GSS transcripts were lower, MT2A was lower, and TJP1 was lower (18, 19). These are transcript changes in an iPSC model, not demonstrated collapse of glutathione synthesis or barrier failure in tissue. APOE was lower in A79V (−3.37 log_2 fold-change) and higher in L150P (+1.71). EPHX2 was higher in L150P (+1.54) and not significant in A79V on the isogenic contrast. Soluble epoxide hydrolase inhibitors improve cognition in animal models (20-22); that literature does not establish a protective or harmful EPHX2 direction in human AD.

The practical point is methodological: an aggregate hit rate can conceal opposing mutation-specific transcript directions. These differences are not a basis for mutation-tailored treatment in carriers.

Gene	A79V	L150P	AD Tissue Range	Interpretation
APOE	−3.37	+1.71	—	Opposite transcript directions in the two isogenic contrasts; APOE is an established AD locus
GSS	−0.31	−0.26	−0.13 to −0.98	Lower in both isogenic contrasts and in the tissue range shown
GCLC	−0.53	−0.34	−0.05 to −0.91	Lower in both isogenic contrasts
GCLM	−1.11	−0.42	+0.30 (GSE132903)	Lower in both isogenic contrasts; some tissue contrasts differ in sign
MT2A	−2.02	−2.09	+0.51 to +0.63	Lower in both isogenic contrasts; higher in the listed sporadic-tissue range
MT1X	−0.60	−0.88	—	Lower in L150P; A79V not significant on the panel rule
TJP1	−0.94	−0.90	+0.12 to +0.31	Lower TJP1 transcript in both isogenic contrasts; barrier function not measured
TJP2	−0.85	+0.45	+0.08 to +0.22	Opposite transcript directions in the two isogenic contrasts
EPHX2	−0.76	+1.54	—	Opposite transcript directions in the two isogenic contrasts
SOD2	−0.03	−0.49	−0.15 to +0.42	Lower in L150P only; A79V not significant on the panel rule

Table 5. PSEN1 mutation-specific panel-gene patterns. Values are log_2 fold-change from the isogenic mutant-versus-gene-corrected contrast. An em-dash indicates the gene did not reach the panel-restricted threshold.

Published genetic-variant architecture

Expression levels reflect current pathway activity; genetic variants determine baseline enzyme capacity. Table 6 catalogues published variants relevant to detoxification function in AD, including APOE (25-27), GSTM1 and GSTT1 null alleles (5-7), MTHFR C677T (28, 29), and SOD2 Ala16Val (30, 31). Odds ratios are taken from the cited source studies and are not re-estimated here. Frequencies shown are for European-ancestry populations and vary substantially by population.

Gene	Variant	Effect	Frequency	AD Association
APOE	ε4 allele	Reduced Aβ clearance	14–15%	OR 3–4 (het), 12–15 (hom) (25-27)
GSTM1	Null (deletion)	No enzyme produced	~50%	OR 1.2–1.8 (5-7)
GSTT1	Null (deletion)	No enzyme produced	20–40%	OR ~1.3; synergistic with GSTM1 null
GSTP1	Ile105Val (rs1695)	Altered substrate specificity	~30% Val	OR ~1.3
MTHFR	C677T (rs1801133)	70% decreased activity (TT)	10–15% TT	OR 1.5–2.0 (28, 29)
SOD2	Ala16Val (rs4880)	30–40% decreased mito import	~50% Val	OR 1.2–1.5 (30, 31)
GPX1	Pro198Leu	Reduced activity (Leu)	~30% Leu	OR ~1.3 in some studies
HFE	H63D (rs1799945)	Iron overload	10–15%	OR ~1.4
PON1	Q192R (rs662)	Altered substrate specificity	~30% R	OR 1.2–1.4
NQO1	C609T (rs1800566)	No enzyme (TT)	4–20% TT	OR ~1.2 (28, 29)

Table 6. Published genetic variants affecting detoxification enzyme capacity. OR = odds ratio for AD as reported in the cited source. This table is descriptive and does not establish clinical validity of any research construct.

Research constructs: GVI, DDI, and IDRS

To quantify genetic burden I define the Genetic Vulnerability Index (GVI):

GVI = Σ ln(OR_i) for all deleterious variants carried; cumulative OR = e^GVI

where OR_i is the published odds ratio for each variant. The cumulative odds ratio is recoverable as e^GVI. For protective alleles (OR < 1), ln(OR_i) is negative, reducing GVI. For population simulation, midpoint ORs were used: APOE ε4 heterozygote (3.5), APOE ε4 homozygote (13.5), GSTM1 null (1.5), GSTT1 null (1.3), MTHFR C677T homozygote (1.75), SOD2 Val/Val (1.35), GPX1 Leu carrier (1.3), HFE H63D (1.4), PON1 R allele (1.3), NQO1 C609T homozygote (1.2).

Monte Carlo simulation (n = 10,000; European ancestry frequencies; Hardy–Weinberg equilibrium) yielded a median GVI of 0.71 (95% CI: 0.68–0.74; cumulative OR = 2.03). The 90th percentile GVI was 1.96 (cumulative OR = 7.09), and the 95th percentile was 2.26 (cumulative OR = 9.58). Notably, 64% of simulated individuals had GVI between 0.0 and 1.0, while 9% exceeded 2.0.

The Integrated Detoxification Risk Score (IDRS) combines the two vulnerability axes:

IDRS = GVI + DDI/10

The DDI (a percentage, 0–100) is divided by a scaling constant k = 10 so that its observed range (roughly 7–30%) maps onto 0.7–3.0, matching the empirical GVI range of approximately −2 to +3 and giving the two axes comparable weight by construction. This scaling is a modeling choice, not a calibrated clinical weighting.

As a worked example: an individual carrying APOE ε4 heterozygous (OR 3.5) plus GSTM1 null (OR 1.5) has GVI = ln(3.5) + ln(1.5) = 1.25 + 0.41 = 1.66, corresponding to cumulative OR = e^1.66 ≈ 5.25 (i.e., 3.5 × 1.5). With DDI = 50%, IDRS = 1.66 + 50/10 = 6.66, compared to IDRS = 1.66 + 0 = 1.66 for the same genetic profile with normal expression.

The “double hit” effect is illustrated by comparing three scenarios: Person A (GVI = 0, DDI = 20%) had IDRS = 0 + 20/10 = 2.00; Person B (GVI = 1.66, DDI = 0%) had IDRS = 1.66 + 0 = 1.66; Person C (GVI = 1.66, DDI = 20%) had IDRS = 1.66 + 20/10 = 3.66. Person A—a sporadic, non-genetic profile with no deleterious variants—still receives IDRS = 2.00, exceeding Person B’s purely genetic score. This directly illustrates that acquired expression dysregulation is a co-equal vulnerability axis rather than a mere multiplier of genetic risk. A multiplicative formulation would assign Person A a score of zero, which would be implausible for the sporadic AD phenotype that accounts for the majority of cases.

The IDRS distribution shifts substantially with increasing DDI. At DDI = 0%, the median IDRS was 0.71 (identical to GVI). At DDI = 50% (severe dysregulation), the median IDRS increased to 5.71. At DDI = 41.2% (panel-basis RNA-seq peak, Aβ-microglia 24 h), the median IDRS reached 4.83 (GVI median 0.71 + 41.2/10); at the 90th GVI percentile (1.96) it reached 6.83. These values describe how the score behaves when high genetic burden and high tissue dysregulation coincide; they are not empirical risk estimates, since a maximal tissue DDI (postmortem or in-vitro brain) would not be measurable in a living individual. Sensitivity analysis confirmed robustness: four alternative GVI weighting schemes (squared-effect, binary count, pathway-weighted, APOE-dominant) all correlated strongly with the base model (r = 0.76–0.99), indicating that the same simulated individuals are ranked highest on the index regardless of weighting approach.

Genetic vulnerability is stratified by GVI (Low < 0.5, Moderate 0.5–1.5, Elevated 1.5–2.5, High > 2.5, corresponding approximately to the population median through the top 5%), and expression vulnerability by the DDI severity bands. All thresholds are provisional and require prospective validation against clinical outcomes before any clinical application.

The Detoxification Dysregulation Index is the per-dataset descriptive measure defined above; the absolute $\log_2$ fold-change floor of 0.5 belongs to the DDI alone and is not part of the locked high-confidence rule, which has no fold-change floor. All three constructs are uncalibrated. They are not

diagnostic, prognostic, treatment-selection, or treatment-response tools, and no threshold reported here has been validated against a clinical outcome.

DISCUSSION

The principal observation of this analysis is compartmental discordance. Applying one locked panel and one rule across brain, liver, and blood shows that detoxification-related transcripts do not move in a single direction in Alzheimer's disease, and that the three compartments do not even engage the same parts of the panel. Brain shows metal-handling induction against reduced glutathione-synthesis and thioredoxin abundance, with median I^2 among high-confidence genes of 79.3%, so pooled cerebral effects should be read with that heterogeneity in view. Liver shows a bile-acid and steroidogenic signature. Blood shows a predominantly mitochondrial profile.

This is a different picture from the one that a brain-only analysis produces, and it constrains interpretation in a useful way. A uniform-failure model of detoxification in AD is not supported by these data. Whatever is happening centrally is not simply a local instance of a systemic deficit.

A sterol-disposal signal within the detoxification panel

One point of orientation before the findings. Sterol elimination is a detoxification function in the sense this panel enumerates. The panel was built by complete functional-family enumeration of the machinery by which cells and organs modify and clear lipophilic compounds, and the cytochrome P450 families that hydroxylate cholesterol are members of exactly that machinery: the body cannot excrete cholesterol as such, and disposes of it only after enzymatic hydroxylation to bile acids or oxysterols. The genes described below are therefore not a departure from the detoxification frame but a specific and unanticipated result within it — the conjugation and clearance machinery applied to an endogenous rather than a xenobiotic substrate.

The result with the widest support in this analysis is not the hepatic one. Three genes of the cholesterol-to-oxysterol-to-bile-acid pathway meet the locked high-confidence rule in the six-cohort brain meta-analysis, each informative in every cohort: CYP46A1 down, CYP27A1 up, CYP39A1 up. CYP46A1 is cholesterol 24-hydroxylase. Brain cholesterol is synthesised locally and is separated from the circulating pool by the blood-brain barrier, so it cannot be exported as cholesterol; conversion to 24S-hydroxycholesterol by CYP46A1 is the quantitatively dominant route by which the brain eliminates it at all (55). Lower CYP46A1 transcript abundance, with higher CYP27A1 and CYP39A1 transcripts, is the observed pattern in that route; it does not establish reduced enzyme capacity or altered sterol flux. Six independent cohorts, direction-concordant, under a rule fixed before the analysis.

The hepatic contrast is the peripheral counterpart of the same problem, and its two genes are one finding rather than two. CYP7A1 and CYP17A1 both act on cholesterol-derived substrate and send it to opposite fates. CYP7A1 is cholesterol 7α-hydroxylase, the rate-limiting and flux-controlling first step of the classical bile-acid synthesis pathway, which is the principal route by which the body as a whole

eliminates cholesterol. CYP17A1 is the 17α-hydroxylase and 17,20-lyase that diverts cholesterol-derived pregnenolone into steroid-hormone synthesis. Read together, the hepatic signature is cholesterol directed toward catabolism and excretion and away from steroidogenic conversion.

Taken as a pair, the two compartments are not engaging unrelated parts of the panel. They are engaging one pathway — cholesterol to oxysterol to bile acid — at the two points where each organ controls it: lower export-enzyme transcript abundance centrally, higher rate-limiting-synthase transcript abundance peripherally. That is a specific, directional and anatomically coherent claim, and it is also falsifiable in a way the earlier xenobiotic framing was not, because it predicts particular oxysterol and bile-acid species in particular compartments rather than a general direction of change across a gene family. The central arm carries the weight: high-confidence calls in six independent cohorts, against twelve donors on the hepatic side.

The hepatic magnitude belongs to CYP7A1. A pooled $\log_2$ fold-change of + 5.65 at $Q = 1.5 \times 10^{-6}$ corresponds to roughly a fiftyfold increase in transcript abundance for the enzyme that sets flux through the pathway. CYP7A1 is under negative feedback from the bile-acid pool returning through the enterohepatic circulation, by way of intestinal FXR and FGF19, so a large increase in its message is what a liver does when that returning pool is depleted rather than when bile-acid synthesis is proceeding normally.

That matters because the established Alzheimer's bile-acid literature points the other way. In the Alzheimer's Disease Neuroimaging Initiative cohort (n = 1,464), cholic acid was lower in Alzheimer's disease, secondary bile acids were higher, and the ratio of deoxycholic to cholic acid was associated with diagnosis at $P = 1.53 \times 10^{-8}$, replicated in an independent cohort; lower cholic acid and a higher ratio also predicted progression from mild cognitive impairment over about four years (48). The same bile-acid measures track neuroimaging and cerebrospinal-fluid biomarkers (51), and metabolic network analysis finds bile-acid synthesis and cholesterol metabolism altered in Alzheimer's brain itself (52). Most directly, lower serum 7α-hydroxycholesterol — the immediate product of CYP7A1 — together with lower cholic and chenodeoxycholic acid, is associated with higher brain amyloid deposition, faster white-matter lesion accumulation, and faster brain atrophy, predominantly in men (53).

The hepatic transcript reported here and those circulating metabolites are therefore discordant in a specific and informative way: the rate-limiting message is up while the pathway's products are down. Two readings are available and these data do not separate them. The first is compensatory de-repression — a depleted bile-acid pool releasing CYP7A1 from feedback inhibition, so that the induction is a consequence of low flux rather than a cause of high flux. The second is a block downstream of transcription, at enzyme abundance, cofactor availability, or hepatic free-cholesterol supply, so that message rises without product following. Both describe a pathway being pushed and not delivering, which is a more specific hypothesis than either the transcript or the metabolite data generate alone.

A pharmacological observation is consistent with taking that state seriously rather than reading it as benign compensation. Bile-acid sequestrants interrupt enterohepatic recirculation, deplete the bile-acid

pool, and de-repress CYP7A1 — producing, in outline, the same configuration seen here. In a primary-care cohort comparing 3,208 sequestrant users with 23,483 users of other non-statin lipid-modifying therapy, sequestrant exposure was not associated with all-cause dementia (HR 1.03, 95% CI 0.72–1.46), but showed a significant dose–response relationship with vascular dementia in men (p for trend = 0.045; HR 2.89, 95% CI 0.96–8.68) and none in women (53). The confidence interval crosses unity, the event counts are small, confounding by indication is unaddressed, and no causal claim is warranted. What is notable is the direction and the sex-specificity, which match the metabolomic arm of the same study rather than opposing it.

This bears on a wider confusion. Circulating cholesterol concentration is routinely treated as though it indexed Alzheimer's risk directly, but the epidemiology does not behave that way: high total cholesterol in midlife is associated with later dementia (61), while high total cholesterol in late life is associated with reduced dementia incidence (62), a reversal more consistent with declining cholesterol being an early feature of the disease process than with the lipid level being the operative variable. The framework here suggests why a pool measurement would behave inconsistently. Plasma cholesterol does not cross the blood-brain barrier; the compartments communicate through oxysterol flux, outward as 24S-hydroxycholesterol and inward as 27-hydroxycholesterol (55). A serum cholesterol concentration therefore reports the size of a pool that the brain does not draw on, while the transcripts altered here govern the rate at which cholesterol leaves each compartment. Pool size and disposal rate are different quantities and need not move together.

The same distinction may be why interventions on cholesterol have produced an inconsistent cognitive literature. Statins act on synthesis, largely peripherally, and differ among themselves in blood-brain barrier penetration; bile-acid sequestrants act on the disposal route, and are the class for which a dementia signal was actually observed (53). Consistent with a disposal-rate rather than pool-size model, the one intervention aimed directly at cerebral cholesterol turnover has shown target engagement: low-dose efavirenz, a CYP46A1 activator, raised plasma and cerebrospinal fluid 24-hydroxycholesterol and increased brain cholesterol turnover 2.5-fold in a placebo-controlled pilot in early Alzheimer's disease, albeit in five participants (63). Nothing in the present transcript data tests any of these agents, and this paragraph is offered as an interpretive frame rather than as evidence about treatment. The prediction it makes is nonetheless concrete: measures of cholesterol disposal — 24S-hydroxycholesterol, 27-hydroxycholesterol, 7α-hydroxycholesterol and the bile-acid profile — should carry information about Alzheimer's disease that serum cholesterol concentration does not.

The CYP17A1 result requires a stronger caveat than the CYP7A1 result and should not carry interpretive weight on its own. CYP17A1 is adrenal- and gonad-enriched, expressed at high levels in adrenal cortical and Leydig cells and only detected, not enriched, in liver. A reduction of this magnitude in twelve livers, on a gene with low hepatic baseline expression, is a flag rather than a finding, and it is not evidence about systemic steroid production. The reason it is nonetheless worth recording is anatomical: CYP17A1 is the single gate to both steroid branches, its 17α-hydroxylase activity providing the obligatory entry to cortisol and its 17,20-lyase activity the entry to dehydroepiandrosterone and thence to androgens and

estrogens. Reduced CYP17A1 would shift flux away from both and toward the mineralocorticoid and progesterone-derived branches. Glucocorticoid involvement in Alzheimer's disease is independently established, with higher cortisol associated with dementia risk, disease severity, and rate of decline (54). Whether hepatic steroidogenic transcripts have any bearing on that is untested, and nothing here tests it.

The experiment that would resolve the central question is a metabolite measurement rather than another transcript comparison. Measuring 24S-hydroxycholesterol and 27-hydroxycholesterol in brain, and 7α-hydroxycholesterol, cholic acid, chenodeoxycholic acid and the deoxycholic-to-cholic ratio in liver or matched serum, would establish whether the transcript changes reported here are accompanied by altered pathway flux or by depleted product. A finding of message up with product down would constitute evidence of a functional block in the principal route of cholesterol elimination in Alzheimer's disease. The cerebral half of that test is available now without new tissue: cohorts holding both brain transcriptomics and brain metabolomics on the same donors would allow CYP46A1 expression to be related to 24S-hydroxycholesterol within individuals, which the present between-group design cannot do.

Inflammation, cortisol, and what this panel cannot see

Elevated inflammatory markers and elevated cortisol are both associated with Alzheimer's disease risk, which is superficially contradictory because glucocorticoids are anti-inflammatory. The standard resolution is glucocorticoid receptor resistance. Sustained inflammatory signalling drives the hypothalamic-pituitary-adrenal axis chronically; prolonged cortisol exposure then desensitises glucocorticoid receptor signalling in immune cells, so cortisol continues to rise while ceasing to restrain inflammation. That coupling — chronic stress, receptor resistance, uncontrolled inflammation, disease risk — has been demonstrated directly (56). The two observations are one dysregulated loop rather than two competing explanations, and the loop is feed-forward rather than self-limiting.

Both measures also index much besides the disease. Chronic inflammatory load rises with age and is shaped by lifelong infectious, nutritional, and metabolic exposure (8), and cortisol tracks visceral adiposity, sleep fragmentation, depression, and glycaemic dysregulation. Each of those is separately associated with dementia risk, so a correlation between either marker and Alzheimer's disease is compatible with both being consequences of a shared upstream state rather than steps in a causal chain.

Whether either is causal for Alzheimer's disease is a separate question, and the genetic evidence is not encouraging for the systemic-inflammation reading. In a Mendelian randomization study of twelve immune-cell measures and five signalling molecules including C-reactive protein, interleukin-6, fibrinogen, and lipoprotein-associated phospholipase A2, no genetically predicted exposure was associated with Alzheimer's disease risk or with hippocampal volume after correction for multiple testing (57). Meanwhile the disease's own common-variant architecture points repeatedly at myeloid and microglial genes. The word inflammation is therefore doing two jobs in this literature: one for central innate immunity, which the genetics supports, and one for circulating inflammatory tone, which it does not. Observational studies mostly measure the second and are commonly read as evidence for the first.

Cortisol carries an additional problem of direction. The hippocampus and medial prefrontal cortex supply the glucocorticoid-receptor-mediated negative feedback that terminates the stress response, and those are among the structures Alzheimer's disease destroys first. Higher cortisol in established disease is therefore expected as a consequence of neurodegeneration, independently of any causal contribution it may make to it (58). Cross-sectional associations between cortisol and tau, or between cortisol and regional atrophy, fit that direction as comfortably as the reverse.

One connection between this and the hepatic findings is worth stating precisely, because the obvious version of it fails. Bile acids modulate glucocorticoid handling: in cholestasis, 11β-hydroxysteroid dehydrogenase type 2 activity falls, and chenodeoxycholic and deoxycholic acid inhibit that enzyme directly, allowing cortisol to escape inactivation and reach the mineralocorticoid receptor (59, 60). If the relevant variable were total bile-acid pool size, this would point the wrong way for Alzheimer's disease, where classical-pathway products are depleted. But the reported Alzheimer's signature is compositional rather than quantitative — cholic acid lower, deoxycholic acid higher, and the deoxycholic-to-cholic ratio the strongest single discriminator (48) — and deoxycholic acid is one of the two acids shown to inhibit the enzyme. The compositional shift therefore moves the specific species that increases tissue cortisol exposure in the direction that would increase it. This is an extrapolation from cholestatic to physiological concentrations and is offered as a hypothesis, not as a mechanism these data establish.

The limits of the instrument should be stated plainly here, because they bear directly on this section. The locked panel contains neither HSD11B1 nor HSD11B2, and it contains neither the glucocorticoid receptor NR3C1 nor its co-chaperone FKBP5. It also contains neither of the bile-acid receptors, the nuclear receptor NR1H4 and the membrane receptor GPBAR1, through which bile acids exert most of their anti-inflammatory effects. The glucocorticoid-regeneration axis, the receptor-sensitivity axis, and the bile-acid signalling axis are consequently invisible to this analysis, and nothing reported here constitutes evidence about any of them. They are named because they are the natural content of a subsequent panel version, not because they were tested and found unremarkable.

Sex dimorphism

The male-associated hepatic CYP26B1 observation is the most fragile in this analysis and the one most likely to be spurious at n = 12; the broader "male-predominant compensatory clearance" reading is not made here, because the other cytochromes that seemed to support it reach significance only against the two male control livers. The CYP26B1 observation is retained because hepatic CYP expression is known to be sex-dimorphic in humans and because late-life AD incidence shows a female excess, so the pairing is at least biologically coherent. It is not evidence for a mechanism. It is a reason to power a future hepatic study for sex (34).

Relationship to the published two-phase study

The liver samples and several of the archived series analyzed here were reported previously under a 203-gene panel (4). The present analysis differs in instrument, in statistical framework, and in question. The overlap is stated explicitly so that readers can identify what is new: the locked 468-gene panel, the six-

cohort random-effects meta-analysis under a pre-specified high-confidence rule, and the cross-compartment directional comparison. Reproduction of the earlier MT2A and GSS directions under the new panel and rule is reported as internal replication, not as a new finding.

Genetics and expression as separate layers

Genetic variants and transcript abundance are treated here as distinct observational layers rather than as inputs to a validated joint measure. Adding a GSTM1-null genotype to a lower GSS transcript is a numerical illustration, not a measured joint risk. Whether panel-restricted transcript burden correlates with Braak stage or ATN category is untested (40). ROSMAP or ADNI could test whether any panel-restricted transcript summary adds information to existing AD models (49, 50); that test has not been performed.

Because the constructs are stated but not validated, it is worth specifying what validating them would require, so that the claim can be tested rather than merely qualified. It needs a cohort holding three things at once: genotypes at the admitted variant positions, a tissue measurement from which a per-sample DDI can be computed, and prospective clinical outcomes. Given that, five questions follow in order. Do the DDI severity bands, which are currently derived from the distribution of observed values, correspond to anything when calibrated against outcomes rather than against each other? Does the GVI add information beyond APOE genotype alone, and beyond a contemporary genome-wide polygenic score? Does any panel-restricted expression summary improve discrimination and calibration over an existing model built from age, sex, APOE, and that polygenic score — measured as change in the concordance statistic and in net reclassification, not as a significant association? Is the scaling constant in the IDRS replaceable by a weight fitted to data, since its present value is a convention chosen to make two ranges comparable? And does the whole thing behave the same way in non-European ancestry, where the allele frequencies and several of the published odds ratios differ?

The third of those questions is the one that decides whether the constructs have any future. A risk index that is significantly associated with disease but adds nothing to a model a clinician could already build is not useful, and this analysis provides no evidence either way. There is also a prior obstacle specific to the expression term: the DDI values that are largest here come from postmortem brain and from in-vitro systems, neither of which can be measured in a living person, so a deployable index would have to be built on an accessible tissue. Whether a blood-derived DDI carries usable information, rather than reflecting the central signal too weakly to matter, is untested and is the first thing that should be established. Cohorts such as ROSMAP and ADNI hold the genotype, expression, and longitudinal outcome data these questions require (49, 50), and running them there is a direction of work in its own right, independent of the sterol findings reported above.

The hardware-and-software framing

The two layers can be pictured as baseline capacity and current activity (Fig. 2). The illustration below is a way of describing that distinction; it is not a measured joint risk and no such joint measure is validated

here.

Consider three hypothetical individuals: Individual X carries normal GSTM1 but shows GSS downregulation—they retain genetic capacity for recovery. Individual Y carries GSTM1 null but shows normal GSS expression—they compensate through alternative pathways. Individual Z carries GSTM1 null AND shows GSS downregulation—they face a “double hit” with compromised genetics and failing compensation. The illustration is descriptive only. It is not a basis for treatment selection.

Mutation-specific therapeutic implications

The A79V and L150P isogenic contrasts differ at specific panel genes, so an aggregate hit rate can hide mutation-specific transcript patterns. Those differences are not a basis for mutation-tailored treatment in carriers.

Integration with established AD staging systems

Whether panel-restricted transcript burden correlates with Braak stage or ATN category is untested (40). Cholinergic, anti-infective, prevention and supplementation hypotheses that the earlier study discussed (4) and that are developed elsewhere (41–47) are not part of this preprint.

The APOE-cysteine-glutathione hypothesis

The APOE risk allele's contribution may be partially mediated through detoxification capacity (25–27). The three APOE isoforms differ in cysteine content: APOE2 contains two cysteine residues, APOE3 one, and APOE4 none (35, 36). Cysteine is rate-limiting for glutathione synthesis (37). If the cysteine-content hypothesis were confirmed at the metabolite level, APOE risk-allele carriers would be a rational group in which to measure glutathione and to test precursor supplementation (38, 39). The transcript data reported here do not confirm that prediction and are not evidence for supplementation in any group.

LIMITATIONS

The hepatic cohort is small. Twelve samples (7 AD, 5 control) cannot support generalizable inference, and the sex-stratified hepatic comparison rests on three to four donors per group. Every hepatic and sex-stratified statement in this analysis is hypothesis-generating and is labelled as such. Replication in an adequately powered, clinically annotated liver series is required before any of it should be built upon.

The bio-banked hepatic samples carry unmeasured confounding. Agonal state, post-mortem interval, medication exposure, hepatic comorbidity, nutritional status, and terminal illness all plausibly affect hepatic CYP transcript abundance and are not controlled here. A compensatory-clearance interpretation and an advanced-dementia-metabolic-change interpretation are not distinguishable in these data, and the provenance of the collection — an oncological research centre — makes malignancy, cachexia, and oncological treatment exposure specific and plausible confounders of hepatic cytochrome P450 transcript abundance in this series. The recorded causes of death differ systematically between the groups: the Alzheimer's donors died of Alzheimer's disease with cerebral edema, pneumonia, or

cachexia, while every control died of cardiovascular disease or pulmonary embolism. Terminal illness of those two kinds plausibly affects hepatic transcription in different ways, and this cannot be separated from diagnosis in these data.

Transcript abundance does not establish protein abundance, enzymatic activity, cellular flux, barrier function, or causal pathway engagement. This applies to all three compartments and is especially relevant to the cytochrome P450 findings, where activity rather than message is the functionally meaningful quantity.

Brain heterogeneity is high. Median I^2 among high-confidence genes was 79.3%, reflecting differences in region, platform, disease stage, and cellular composition across the six cohorts. Pooled brain estimates should be read with that in mind.

Compartments were not sampled from the same individuals. The brain, liver, and blood data derive from separate donor sets, so within-person compartmental concordance cannot be assessed. The discordance reported here is between-group, not within-subject, and a matched multi-tissue cohort would be the definitive design. Bulk postmortem brain was not cell-type deconvolved, so metallothionein induction and lower neuronal-pump transcripts are compatible with gliosis and neuronal loss as well as with cell-intrinsic change.

The DDI classification thresholds are provisional and derived from distributional properties rather than calibrated against clinical outcomes. The GVI relies on published odds ratios that vary across studies and populations and does not capture epistasis or gene-environment interaction. The IDRS uses an uncalibrated scaling constant.

Diagnosis is completely confounded with collection date in the hepatic series. Every control liver was collected before every Alzheimer's liver — controls between July 2013 and June 2017, cases between September 2017 and September 2019, with no overlap and a median separation of about two years and three months. Storage duration, and any change in banking, handling, or extraction practice across that interval, is therefore perfectly collinear with disease status. No statistical adjustment can separate the two in a design of this shape, and any hepatic difference reported here is a difference between two groups that also differ in when they were collected. The groups are otherwise reasonably matched: mean age 81.4 years in cases against 77.2 in controls, mean post-mortem interval 3.1 against 3.5 hours, mean body-mass index 24.2 against 24.9, and all donors of the same recorded ethnicity.

Several hepatic effect sizes exceed 10 on the log2 scale, including CYP2A13, SULT1E1, CYP4F12, and CYP17A1 at transcript level. Values of that magnitude in a 12-sample experiment indicate that a transcript was effectively undetected in one group rather than graded between groups, and they are sensitive to a single donor. They are reported where the source study reported them, but no interpretive weight is placed on their magnitude, and the primary hepatic result is confined to the gene-level all-case against all-control contrast.

The sex-stratified hepatic contrasts have two to four donors per cell, and the male control group contains two livers. Any comparison drawn against that group is determined by two individuals. This is why the several cytochromes that reach significance only against male controls are reported as exploratory and are not described as a male Alzheimer's signature.

The panel does not cover several axes that bear on the interpretations discussed here. It contains no glucocorticoid-regeneration genes (HSD11B1, HSD11B2), no glucocorticoid-receptor or co-chaperone genes (NR3C1, FKBP5), and neither bile-acid receptor (NR1H4, GPBAR1). It also contains no cytokines, inflammasome components, or microglial receptors, so the single inflammation-associated high-confidence call (NFKB1) should not be read as a characterisation of neuroinflammation in Alzheimer's disease. Absence from the panel reflects the functional-family enumeration used to build it and the fact that it was frozen before these questions arose; it is not evidence of absence of effect.

In a competitive permutation test the panel did not exceed power-matched random gene sets. The DDI therefore reflects transcriptional dysregulation broadly rather than these 468 genes uniquely, and no claim of panel-specific enrichment is made here.

The IDRS has no prospective validation, no demonstrated incremental value over existing AD risk models, and no usable living-brain expression input. iPSC models may not recapitulate in vivo biology. The peripheral blood signature may not directly reflect brain pathology. Cross-dataset comparisons remain subject to batch effects, which within-dataset analysis mitigates but does not eliminate. Generalization beyond European-ancestry populations requires population-specific allele frequencies.

Per-cohort polarity checks for the present AD analysis are reported in the Supplementary Materials. Polarity verification should be treated as standard practice for GEO2R-based meta-analyses.

The primary brain inference is the six-cohort mixed-platform meta-analysis, not an RNA-sequencing-only analysis, and the four microarray cohorts are part of that primary pool rather than a second tier. A residual limitation is that the microarray tier does not fully cover several 468-gene panel members — including APOE, MTHFR, COMT, HFE, SLC40A1, NOS2, VWF, CGN, ACSL4, NCOA4, MB21D1 and TMEM173 — owing to probe coverage, so cross-platform corroboration applies principally to the genes measurable on both platforms.

Only two of the six primary cohorts are RNA-sequencing, and each contributes fewer than thirty subjects. That is a consequence of how few independent adult postmortem Alzheimer's brain RNA-sequencing donor cohorts were publicly archived in GEO and admissible under the locked rule, not of a design preference, and the cohort-count analysis in Results shows that 79.4% of high-confidence genes draw on at least one sequencing cohort. It remains a real constraint. The direct remedy is to extend the primary set to controlled-access resources such as the AMP-AD cohorts, which lie outside the GEO-only search boundary declared in Materials and Methods; doing so would require re-locking the cohort set and is identified here as the next analysis rather than claimed as done.

No enzyme activity, protein, or metabolite measurement was performed in this study, and no prospective clinical outcome was assessed.

CONCLUSIONS

Applying one locked 468-gene detoxification panel to Alzheimer's disease brain, liver, and blood shows that these compartments do not change together. The six-cohort brain meta-analysis yields 458 analyzable panel genes, 167 at FDR < 0.05, and 141 high-confidence genes, with metallothionein induction set against reduced glutathione-synthesis and thioredoxin transcripts. Primary hepatic RNA sequencing (n = 12) is hypothesis-generating and yields a signature on a different axis: bile-acid synthesis and steroidogenesis, with CYP7A1 sharply up and CYP17A1 down, and no coherent direction across xenobiotic-metabolizing cytochromes. Peripheral blood is dominated instead by mitochondrial transcripts.

The supported inference is that detoxification-related transcript change in Alzheimer's disease is compartment-specific, and that conclusions drawn from brain tissue alone should not be generalized to the organism. The hepatic observations rest on 12 samples and are hypothesis-generating. GVI, DDI, and IDRS are research constructs requiring prospective, multi-ancestry validation before any clinical application.

Two lines of work follow from this, and they are independent of one another. The first concerns the sterol-disposal finding. It requires measurement of pathway products rather than transcripts — 24S- and 27-hydroxycholesterol in brain, and 7α-hydroxycholesterol, cholic acid, chenodeoxycholic acid and the deoxycholic-to-cholic ratio in liver or matched serum — together with a larger, clinically annotated hepatic cohort, hepatic protein and enzyme-activity measurement rather than message, and ultimately a matched multi-tissue series in which brain, liver, and blood come from the same individuals. The cerebral half of that programme can begin immediately in existing cohorts that hold brain transcriptomics and brain metabolomics on the same donors.

The second concerns the research constructs, and it is not secondary. GVI, DDI, and IDRS are stated here without validation, and the work that would establish or refute them is specified in the Discussion: calibration of the DDI bands against clinical outcomes rather than against their own distribution; a test of whether the GVI adds information beyond APOE and a contemporary polygenic score; a test of whether any panel-restricted expression summary improves discrimination and calibration over an existing risk model, measured as change in the concordance statistic and net reclassification; replacement of the IDRS scaling convention with a fitted weight; determination of whether an accessible-tissue DDI carries usable information at all; and replication across ancestries. Until those are done the constructs remain research formulae, and no clinical use of them is supported.

MATERIALS AND METHODS

Gene panel

A 468-gene detoxification panel was assembled by complete functional-family enumeration of xenobiotic-detoxification, antioxidant-defense, metal-homeostasis, and barrier-associated machinery, not by data-driven feature selection. Pre-specified, outcome-blind filters removed pseudogenes and ambiguous symbols, and only genes passing a group-blind detection threshold within a dataset were analyzed. Genes were never added or removed on the basis of case-versus-control association. The panel was frozen on 2026-07-06 and is deposited unchanged at https://doi.org/10.5281/zenodo.22178094.

A 40-gene SENSITIVITY layer (proteostasis, mitochondrial-respiratory, and cGAS–STING innate-immune genes) is reported separately as a broader cellular-defense robustness analysis and is not part of the AD CORE analysis. The panel was reconciled with the XenoReg detoxification and physiological-barrier gene set of Santos et al. (64), 519 genes, as conceptual basis.

For the GVI, variants were admitted under a tiered minor-allele-frequency and effect-size framework: Tier 1, common variants with MAF at or above 1% in any major reference population; Tier 2, rare but actionable variants below 1% MAF meeting an FDA or ACMG–ClinGen actionability standard or a robust effect size (OR at or above 2, or protective OR at or below 0.7). Defining Tier 1 by frequency in any major population rather than in Europeans alone limits Eurocentric ascertainment bias.

Brain cohorts and meta-analysis

Six independent postmortem adult-brain GEO cohorts were admitted to the primary meta-analysis: GSE33000 (16), GSE132903 (17), GSE5281, and GSE48350 (microarray) and GSE173955 (14) and GSE159699 (13) (RNA-seq). Inclusion required at least three samples per group and a standard DESeq2 or limma pipeline. Differential expression used PyDESeq2 for RNA-seq and limma with empirical Bayes moderation for microarray, with Benjamini–Hochberg correction computed within the 468-gene panel.

For GSE48350 the analyzed contrast was Braak stage IV or greater versus neuropathologic code-C controls (61 versus 140). Platform was treated as a pre-specified source of between-cohort heterogeneity rather than as a reason to exclude a cohort, so the four microarray cohorts in the locked set are primary and contribute per-gene effect sizes to the 167 and 141 counts.

The platform composition of the primary set follows from the eligibility rule rather than from a preference for either technology. Admission required an independent, adult, postmortem human brain series comparing Alzheimer's disease with control, at least three samples per group, panel-mappable annotation, and no donor overlap with an already admitted series. Applied to the RNA-sequencing series analyzed in this work, that rule admits exactly two. GSE211993 is iPSC-derived neurons and GSE227221 is cultured microglia under amyloid-beta exposure, so neither is postmortem tissue; GSE190125 is whole blood from trisomy 21 donors, so it is neither brain nor Alzheimer's disease; and GSE153873 and GSE104704 are transcriptomic arms of the same investigator cohort as the admitted series GSE159699,

so both are excluded by the de-duplication rule. The two admissible RNA-sequencing cohorts, GSE173955 and GSE159699, come from different studies and different donor populations. The constraint is therefore on the number of independent adult postmortem Alzheimer's brain RNA-sequencing donor cohorts that were publicly archived in GEO and admissible under the locked rule, not on the use of RNA sequencing.

The search boundary is stated so that it can be checked. Candidate series were those publicly archived in the NCBI Gene Expression Omnibus and retrievable without a data-use agreement, as of the panel-lock date of 2026-07-06. Large controlled-access resources — including the AMP-AD cohorts distributed through the Synapse portal — were outside that boundary and were not screened. Extending the primary set to those resources is the most direct way to increase the RNA-sequencing contribution and is identified in the Limitations as the next step rather than claimed as done.

Per-gene effect sizes were combined by inverse-variance random-effects meta-analysis (DerSimonian–Laird) using reported standard errors, with mean-probe collapse and no significance-based probe selection. The locked high-confidence rule requires FDR < 0.05, measurement in at least three cohorts, direction-concordance in at least 70% of cohorts, and nominal significance ($P < 0.05$) in at least two cohorts. Between-cohort heterogeneity is reported as I^2.

The two admitted sequencing cohorts are independent of one another in study, region, and population. GSE173955 (Kyushu University) comprises postmortem hippocampus from 8 Alzheimer's disease and 10 non-Alzheimer's subjects donated to the Hisayama study, sequenced on an Illumina HiSeq 1500. GSE159699 (University of Pennsylvania) comprises postmortem lateral temporal lobe from Alzheimer's disease, aged-control, and young-control donors, sequenced on an Illumina NextSeq 500.

The GSE173955 depositors note that one Alzheimer's and one non-Alzheimer's library was run twice on the sequencer to obtain additional reads. That repeat run is a depth-acquisition step and not a second observation: the source publication reports expression profiling of hippocampal RNA from 10 non-Alzheimer's and 8 Alzheimer's subjects, one profile per subject (14). The analysis unit here is likewise the subject: where a repository holds more than one sequencing run for a single library, those runs are treated as one observation from one donor and their counts summed before differential expression, rather than entered as independent samples.

Panel-restricted differential expression was recomputed here from the repository count matrices under one uniform pipeline rather than carried over from the depositing authors' own analyses, which used study-specific tools and thresholds — StringTie with edgeR likelihood-ratio testing in the case of GSE173955 (14). Reusing published per-study calls would have mixed inference rules across cohorts and made the pooled estimate uninterpretable.

Two further sequencing series from the same investigator group as GSE159699 were screened and not admitted, under the pre-specified rule that no two primary cohorts may share donors. GSE153873 is, with GSE159699, a sub-series of SuperSeries GSE153875 — both are transcriptomic arms of the same study

and publication. GSE104704 is the predecessor study from the same group, sampling the same brain region on the same sequencing platform under the same Alzheimer's, aged-control, and young-control design, so donor overlap with GSE159699 cannot be excluded. Admitting either would have risked duplicate donor representation in the pool.

Treating GSE153873 as a within-cohort contrast rather than as an independent seventh cohort also strengthens its use as the aging-specificity control reported in Results: because the near-null aging comparison is drawn from the same study as one of the primary cohorts, its near-null result cannot be attributed to between-cohort differences in platform, region, or donor ascertainment.

Note on the GSE159699 record. The GEO summary field for GSE159699 describes hippocampus while its overall-design field describes postmortem lateral temporal lobe; the associated publication and the predecessor series GSE104704 both concern lateral temporal lobe, and the region is recorded as lateral temporal lobe throughout this manuscript. Third-party mirrors of the GEO record propagate the summary field and may therefore appear to disagree.

Hepatic tissue and RNA sequencing

Human liver tissue from 7 Alzheimer's disease donors and 5 controls (12 samples) was obtained commercially from AMSBIO (Cambridge, Massachusetts, USA). Collection of the samples was approved by the Ethics Committee of the N. N. Blokhin Russian Oncological Research Center (PG-ONC 2003/1). All specimens were de-identified and were obtained with informed consent. Donor-level sex, age, ethnicity, autopsy date, post-mortem interval, body-mass index, and cause of death were supplied with the specimens and are reproduced in Table 2. Cases and controls are comparable in age, post-mortem interval, and body-mass index, but not in collection date, which separates the groups completely; this is addressed in the Limitations.

RNA extraction, library preparation, sequencing, and the primary differential-expression analysis were performed by LC Sciences (Houston, Texas, USA), and the procedure is reported in full in the supplementary material of the source study (4). RNA integrity was assessed on an Agilent 2100 Bioanalyzer. Ribosomal RNA was depleted and the remaining RNA fragmented in divalent-cation buffer at elevated temperature; libraries were prepared with Illumina's TruSeq Stranded Total RNA protocol and quantified on an Agilent 2100 Bioanalyzer High Sensitivity DNA chip. Paired-end sequencing was performed on an Illumina NovaSeq 6000; per-sample read length, yield, and quality metrics are held in the sequencing provider's quality-control report and are available from the author on request. Adapter contamination and low-quality or undetermined bases were removed with Cutadapt and in-house Perl scripts, and read quality was verified with FastQC. Reads were mapped to the human genome with HISAT2 (Ensembl release v107); transcripts were assembled with StringTie and merged with gffcompare, and expression was estimated with StringTie and ballgown. Differential expression was computed with DESeq2 and edgeR.

One threshold difference between compartments should be stated explicitly. The hepatic differential-expression calls carried forward here used the source study's criterion of FDR ≤ 0.05 with absolute fold change ≥ 2, equivalent to an absolute $\log_2$ fold-change floor of 1.0. That is stricter than the 0.5 floor used for the descriptive per-dataset DDI in the archived series, and stricter than the locked high-confidence rule, which has no fold-change floor at all. Hepatic calls are therefore conservative relative to the central ones, and the cross-compartment directional comparison is not an artifact of a looser hepatic threshold. Panel membership was applied identically in both compartments.

The hepatic sequencing data were made available on request in the source study (4) and are being deposited in the NCBI Gene Expression Omnibus so that the primary data underlying this analysis are independently retrievable. The accession will be added at the first revision of this preprint.

Supporting contrasts

Supporting and secondary contrasts (GSE211993 (11), GSE227221 (10), GSE190125 (12), GSE63060 (32), GSE153873 (13)) were analyzed under the same panel and significance definition but were not entered into the six-cohort meta-analysis. GSE153873 old-versus-young served as an aging-specificity control. One microarray series (GSE108000) was excluded because its export lacked platform gene-symbol annotation and could not be mapped to the panel.

Research constructs

DDI, GVI, and IDRS are defined in Results and in the deposited methods note. The absolute $\log_2$ fold-change floor of 0.5 applies to the DDI only and is not part of the high-confidence rule, which has no fold-change floor.

DDI_panel is the count of differentially expressed panel genes divided by 468 and multiplied by 100; DDI_measurable uses the measurable denominator. A gene counts as differentially expressed for this index at Benjamini–Hochberg adjusted $P < 0.05$ with absolute $\log_2$ fold-change at or above 0.5, computed within the 468-gene panel. Total Dysregulation Magnitude (TDM) is the sum of absolute $\log_2$ fold-change across significant genes and captures effect size independently of gene count. The two analyses use different pipelines by design, and this should not be read as an inconsistency: the primary six-cohort meta-analysis pools PyDESeq2 and limma effect sizes with their reported standard errors, whereas the descriptive per-dataset DDI and TDM values were computed with GEO2R, which implements limma with empirical Bayes moderation (65), under Benjamini–Hochberg correction (66). Population simulation used Monte Carlo sampling with n = 10,000. The IDRS used here is the raw additive combination GVI + DDI/10; a z-score composite of GVI and DDI is a different construct and is not used in this preprint.

ETHICS AND HUMAN SUBJECTS

The archived transcriptomic analyses used only publicly available, de-identified gene-expression data from the NCBI Gene Expression Omnibus; those datasets carry the ethical oversight of their originating studies. The hepatic analysis used commercially obtained, de-identified human liver tissue purchased from AMSBIO (Cambridge, Massachusetts, USA). Collection of that tissue was approved by the Ethics Committee of the N. N. Blokhin Russian Oncological Research Center (PG-ONC 2003/1), and the samples were obtained with informed consent. No identifiable private information was accessed, and no living human subjects were enrolled, recruited, or intervened upon by the author. The author holds no separate institutional review board affiliation; the applicable oversight is that of the collecting institution named above.

DECLARATION

DECLARATION OF GENERATIVE AI AND AI-ASSISTED TECHNOLOGIES IN THE MANUSCRIPT PREPARATION PROCESS

During the preparation of this work the author used Grok (xAI), Claude (Anthropic), and Perplexity to assist with literature synthesis, bioinformatic pipeline construction, editorial refinement, and critical review of claims and citations. After using these tools, the author reviewed and edited the content as needed and takes full responsibility for the content of the published article.

ACKNOWLEDGMENTS

The author thanks the investigators who generated and deposited the GEO datasets analyzed in this work, and acknowledges the participants in the original studies and the donors whose tissue made the hepatic analysis possible.

FUNDING

This research received no external funding. All work was conducted independently through Sirius Neuroscience, LLC.

AUTHOR CONTRIBUTIONS

M.E.M. conceived the study, curated the 468-gene detoxification panel, obtained and processed all datasets, commissioned and interpreted the hepatic RNA sequencing, performed the statistical analyses and a descriptive population-frequency simulation of the GVI, which is not a risk calculator, created the figures and tables, and wrote the manuscript.

COMPETING INTERESTS

The author is the sole inventor on a filed patent application relating to panel-based research scoring methods that use the locked 468-gene list reported here. The application did not determine gene membership, the high-confidence rule, or the reported results, and the constructs described here are

stated to be unvalidated. Academic reuse of the deposited panel and code does not require a license from the author. The author declares no other competing interests.

DATA AND MATERIALS AVAILABILITY

Archived transcriptomic analyses use publicly available GEO datasets. Primary adult-brain accessions: GSE33000, GSE132903, GSE173955, GSE159699, GSE5281, GSE48350. Supporting accessions: GSE211993, GSE227221, GSE190125, GSE63060, GSE153873. The locked 468-gene panel, excluded-symbol list, GEO accession roles, methods note, and analysis pipeline are deposited at https://doi.org/10.5281/zenodo.22178094. Per-gene meta-analysis results accompany this preprint as Table S3, and the locked panel as Table S2, in the supplementary workbooks. The hepatic RNA-sequencing data are being deposited in the NCBI Gene Expression Omnibus and the accession will be added at the first revision of this preprint; until then they remain available from the author on request, as in the source study.

References

1. World Health Organization (2023) Dementia fact sheet. WHO, Geneva.
2. Scheltens P, De Strooper B, Kivipelto M, Holstege H, Chetelat G, Teunissen CE, Cummings J, van der Flier WM (2021) Alzheimer's disease. Lancet 397:1577–1590. https://doi.org/10.1016/S0140-6736(20)32205-4
3. Alzheimer's A (2023) Alzheimer's disease facts and figures. Alzheimers Dement. 19, 1598–1695 (2023). https://doi.org/10.1002/alz.13016
4. McCaulley ME (2026) Impaired pathways of detoxification and risk of Alzheimer's disease: Differential gene expression studies via gene set expression analysis. J Alzheimers Dis Rep 10:25424823261419382. https://doi.org/10.1177/25424823261419382
5. Piacentini S, Polimanti R, Squitti R, Ventriglia M, Cassetta E, Vernieri F, Rossini PM, Manfellotto D, Fuciarelli M (2012) GSTM1 null genotype as risk factor for late-onset Alzheimer's disease in Italian patients. J Neurol Sci 317:137–140. https://doi.org/10.1016/j.jns.2012.01.026
6. Bernardini S, Bellincampi L, Ballerini S, Federici G, Iori R, Trequattrini A, Ciappi F, Baldinetti F, Bossù P, Caltagirone C, Spalletta G (2005) Glutathione S-transferase P1 C allelic variant increases susceptibility for late-onset Alzheimer disease: association study and relationship with apolipoprotein E ε4 allele. Clin Chem 51:944–951. https://doi.org/10.1373/clinchem.2004.045955
7. Stroombergen MC, Waring RH (1999) Determination of glutathione S-transferase mu and theta polymorphisms in neurological disease. Hum Exp Toxicol 18:141–145. https://doi.org/10.1177/096032719901800302
8. Finch CE (2010) Evolution of the human lifespan and diseases of aging: roles of infection, inflammation, and nutrition. Proc. Natl. Acad. Sci. U.S.A. 107 (Suppl. 1), 1718–1724 https://doi.org/10.1073/pnas.0909606106

9. McCaulley ME (2026) Locked 468-gene detoxification panel, excluded-symbol list, GEO accession roles, methods note, and analysis pipeline. https://doi.org/10.5281/zenodo.22178094. Zenodo
10. Sun N, Victor MB, Park YP, Xiong X, Scannail AN, Leary N et al (2023) Human microglial state dynamics in Alzheimer's disease progression. Cell 186:4386–4403e29. https://doi.org/10.1016/j.cell.2023.08.037
11. Corsi GI, Gadekar VP, Haukedal H, Doncheva A, Anthon S, Ambardar N et al (2023) The transcriptomic landscape of neurons carrying PSEN1 mutations reveals changes in extracellular matrix components and non-coding gene expression. Neurobiol Dis 178:105980. https://doi.org/10.1016/j.nbd.2022.105980
12. Crnic Institute Human Trisome Project (2022) PolyA RNA-seq from whole blood of trisomy 21 and euploid controls, Gene Expression Omnibus accession GSE190125 ;
13. Nativio R, Lan Y, Donahue G, Sidoli S, Berson A, Srinivasan AR et al (2020) An integrated multi-omics approach identifies epigenetic alterations associated with Alzheimer's disease. Nat Genet 52:1024–1035. https://doi.org/10.1038/s41588-020-0696-0
14. Mizuno Y, Abolhassani N, Mazzei G, Sakumi K, Saito T, Saido TC et al (2021) MUTYH actively contributes to microglial activation and impaired neurogenesis in the pathogenesis of Alzheimer's disease. Oxid. Med. Cell. Longev. 8635088 (2021). https://doi.org/10.1155/2021/8635088
15. Sood S, Gallagher IJ, Lunnon K, Rullman E, Keohane A, Crossland H et al (2015) A novel multi-tissue RNA diagnostic of healthy ageing relates to cognitive health status. Genome Biol 16:185. https://doi.org/10.1186/s13059-015-0750-x
16. Zhang B, Gaiteri C, Bodea L-G, Wang Z, McElwee J, Podtelezhnikov AA et al (2013) Integrated systems approach identifies genetic nodes and networks in late-onset Alzheimer's disease. Cell 153:707–720. https://doi.org/10.1016/j.cell.2013.03.030
17. Piras IS, Krate J, Delvaux E, Nolz J, Mastroeni DF, Persico AL et al (2019) Transcriptome changes in the Alzheimer's disease middle temporal gyrus: importance of RNA metabolism and mitochondria-associated membrane genes. J Alzheimers Dis 70:691–713. https://doi.org/10.3233/JAD-181113
18. Zlokovic BV (2008) The blood-brain barrier in health and chronic neurodegenerative disorders. Neuron 57:178–201. https://doi.org/10.1016/j.neuron.2008.01.003
19. Sweeney MD, Sagare AP, Zlokovic BV (2018) Blood-brain barrier breakdown in Alzheimer disease and other neurodegenerative disorders. Nat Rev Neurol 14:133–150. https://doi.org/10.1038/nrneurol.2017.188
20. Hashimoto K (2019) Role of soluble epoxide hydrolase in metabolism of PUFAs in psychiatric and neurological disorders. Front Pharmacol 10:36. https://doi.org/10.3389/fphar.2019.00036
21. Ghosh A, Comerota MM, Wan D, Chen F, Propson NE, Hwang SH, Hammock BD, Zheng H (2020) An epoxide hydrolase inhibitor reduces neuroinflammation in a mouse model of Alzheimer's disease. Sci Transl Med 12:eabb1206. https://doi.org/10.1126/scitranslmed.abb1206
22. Kodani SD, Morisseau C (2019) Role of epoxy-fatty acids and epoxide hydrolases in the pathology of neuro-inflammation. Biochimie 159:59–65. https://doi.org/10.1016/j.biochi.2019.01.020

23. Hidalgo J, Aschner M, Zatta P, Vasak M (2001) Roles of the metallothionein family of proteins in the central nervous system. Brain Res Bull 55:133–145. https://doi.org/10.1016/S0361-9230(01)00452-X
24. Uchida Y, Takio K, Titani K, Ihara Y, Tomonaga M (1991) The growth inhibitory factor that is deficient in the Alzheimer's disease brain is a 68 amino acid metallothionein-like protein. Neuron 7:337–347. https://doi.org/10.1016/0896-6273(91)90272-2
25. Corder EH, Saunders AM, Strittmatter WJ, Schmechel DE, Gaskell PC, Small GW, Roses AD, Haines JL (1993) Pericak-Vance, Gene dose of apolipoprotein E type 4 allele and the risk of Alzheimer's disease in late onset families. Science 261:921–923. https://doi.org/10.1126/science.8346443
26. Farrer LA, Cupples LA, Haines JL, Hyman B, Kukull WA, Mayeux R, Myers RH, Pericak-Vance MA, Risch N, van Duijn CM (1997) Effects of age, sex, and ethnicity on the association between apolipoprotein E genotype and Alzheimer disease. A meta-analysis. APOE and Alzheimer Disease Meta Analysis Consortium. JAMA 278:1349–1356. https://doi.org/10.1001/jama.278.16.1349
27. Belloy ME, Napolioni V, Greicius MD (2019) A quarter century of APOE and Alzheimer's disease: progress to date and the path forward. Neuron 101:820–838. https://doi.org/10.1016/j.neuron.2019.01.056
28. Rai V (2017) Methylenetetrahydrofolate reductase (MTHFR) C677T polymorphism and Alzheimer disease risk: a meta-analysis. Mol Neurobiol 54:1173–1186. https://doi.org/10.1007/s12035-016-9722-8
29. Seshadri S, Beiser A, Selhub J, Jacques PF, Rosenberg IH, D'Agostino RB, Wilson PWF, Wolf PA (2002) Plasma homocysteine as a risk factor for dementia and Alzheimer's disease. N Engl J Med 346:476–483. https://doi.org/10.1056/NEJMoa011613
30. Wiener HW, Perry RT, Chen Z, Harrell LE, Go RC (2007) A polymorphism in SOD2 is associated with development of Alzheimer's disease. Genes Brain Behav 6:770–775. https://doi.org/10.1111/j.1601-183X.2007.00308.x
31. Markesbery WR (1997) Oxidative stress hypothesis in Alzheimer's disease. Free Radic Biol Med 23:134–147. https://doi.org/10.1016/S0891-5849(96)00629-6
32. Lovestone S, Francis P, Strandgaard K (2007) Biomarkers for disease modification trials—the innovative medicines initiative and AddNeuroMed. J Nutr Health Aging 11:359–361
33. Dringen R (2000) Metabolism and functions of glutathione in brain. Prog Neurobiol 62:649–671. https://doi.org/10.1016/S0301-0082(99)00060-X
34. Sudlow C, Gallacher J, Allen N, Beral V, Burton P, Danesh J et al (2015) UK Biobank: an open access resource for identifying the causes of a wide range of complex diseases of middle and old age. PLoS Med 12:e1001779. https://doi.org/10.1371/journal.pmed.1001779
35. Weisgraber KH, Rall SC Jr., Mahley RW (1981) Human E apoprotein heterogeneity: cysteine-arginine interchanges in the amino acid sequence of the apo-E isoforms. J Biol Chem 256:9077–9083. https://doi.org/10.1016/S0021-9258(19)52510-8

36. Dose J, Huebbe P, Nebel A, Rimbach G (2016) APOE genotype and stress response—a mini review. Lipids Health Dis 15:121. https://doi.org/10.1186/s12944-016-0288-2
37. Lu SC (2013) Glutathione synthesis. Biochim Biophys Acta 1830:3143–3153. https://doi.org/10.1016/j.bbagen.2012.09.008
38. Mandal PK, Saharan S, Tripathi M, Murari G (2015) Brain glutathione levels—a novel biomarker for mild cognitive impairment and Alzheimer's disease. Biol Psychiatry 78:702–710. https://doi.org/10.1016/j.biopsych.2015.04.005
39. Pocernich CB, Butterfield DA (2012) Elevation of glutathione as a therapeutic strategy in Alzheimer disease. Biochim Biophys Acta 1822:625–630. https://doi.org/10.1016/j.bbadis.2011.10.003
40. Jack CR Jr., Bennett DA, Blennow K, Carrillo MC, Dunn B, Haeberlein SB et al (2018) NIA-AA Research Framework: toward a biological definition of Alzheimer's disease. Alzheimers Dement 14:535–562. https://doi.org/10.1016/j.jalz.2018.02.018
41. Hampel H, Mesulam MM, Cuello AC, Farlow MR, Giacobini E, Grossberg GT et al (2018) The cholinergic system in the pathophysiology and treatment of Alzheimer's disease. Brain 141:1917–1933. https://doi.org/10.1093/brain/awy132
42. Ferreira-Vieira TH, Guimaraes IM, Silva FR, Ribeiro FM (2016) Alzheimer's disease: targeting the cholinergic system. Curr Neuropharmacol 14:101–115. https://doi.org/10.2174/1570159X13666150716165726
43. Moss DE, Perez RG (2021) Anti-neurodegenerative benefits of acetylcholinesterase inhibitors in Alzheimer's disease: nexus of cholinergic and nerve growth factor dysfunction. Curr Alzheimer Res 18:1010–1022. https://doi.org/10.2174/1567205018666211215150547
44. Moss DE, Perez RG (2024) The phospho-tau cascade, basal forebrain neurodegeneration, and dementia in Alzheimer's disease: anti-neurodegenerative benefits of acetylcholinesterase inhibitors. J Alzheimers Dis 102:617–626. https://doi.org/10.1177/13872877241289602
45. Itzhaki RF, Lathe R, Balin BJ, Ball MJ, Bearer EL, Braak H et al (2016) Microbes and Alzheimer's disease. J Alzheimers Dis 51:979–984. https://doi.org/10.3233/JAD-160152
46. Cairns DM, Rouleau N, Parker RN, Walsh KG, Gehrke L, Kaplan DL (2020) A 3D human brain-like tissue model of herpes-induced Alzheimer's disease. Sci Adv 6:eaay8828. https://doi.org/10.1126/sciadv.aay8828
47. Lovheim H, Gilthorpe J, Adolfsson R, Nilsson L-G, Elgh F (2015) Reactivated herpes simplex infection increases the risk of Alzheimer's disease. Alzheimers Dement 11:593–599. https://doi.org/10.1016/j.jalz.2014.04.522
48. MahmoudianDehkordi S, Arnold M, Nho K, Ahmad S, Jia W, Xie G et al (2019) Altered bile acid profile associates with cognitive impairment in Alzheimer's disease—an emerging role for gut microbiome. Alzheimers Dement 15:76–92. https://doi.org/10.1016/j.jalz.2018.07.217
49. Bennett DA, Buchman AS, Boyle PA, Barnes LL, Wilson RS, Schneider JA (2018) Religious Orders Study and Rush Memory and Aging Project. J Alzheimers Dis 64:S161–S189. https://doi.org/10.3233/JAD-179939

50. Mueller SG, Weiner MW, Thal LJ, Petersen RC, Jack CR, Jagust W, Trojanowski JQ, Toga AW, Beckett L (2005) The Alzheimer's Disease Neuroimaging Initiative. Neuroimaging Clin N Am 15:869–877. https://doi.org/10.1016/j.nic.2005.09.008
51. Nho K, Kueider-Paisley A, MahmoudianDehkordi S, Arnold M, Risacher SL, Louie G et al (2019) Altered bile acid profile in mild cognitive impairment and Alzheimer's disease: Relationship to neuroimaging and CSF biomarkers. Alzheimers Dement 15:232–244. https://doi.org/10.1016/j.jalz.2018.08.012
52. Baloni P, Funk CC, Yan J, Yurkovich JT, Kueider-Paisley A, Nho K et al (2020) Metabolic network analysis reveals altered bile acid synthesis and metabolism in Alzheimer's disease. Cell Rep Med 1:100138. https://doi.org/10.1016/j.xcrm.2020.100138
53. Varma VR, Wang Y, An Y, Varma S, Bilgel M, Doshi J et al (2021) Bile acid synthesis, modulation, and dementia: A metabolomic, transcriptomic, and pharmacoepidemiologic study. PLoS Med 18:e1003615. https://doi.org/10.1371/journal.pmed.1003615
54. Ouanes S, Popp J (2019) High cortisol and the risk of dementia and Alzheimer's disease: A review of the literature. Front Aging Neurosci 11:43. https://doi.org/10.3389/fnagi.2019.00043
55. Bjorkhem I, Meaney S (2004) Brain cholesterol: long secret life behind a barrier. Arterioscler Thromb Vasc Biol 24:806–815. https://doi.org/10.1161/01.ATV.0000120374.59826.1b
56. Cohen S, Janicki-Deverts D, Doyle WJ, Miller GE, Frank E, Rabin BS, Turner RB (2012) Chronic stress, glucocorticoid receptor resistance, inflammation, and disease risk. Proc. Natl. Acad. Sci. U.S.A. 109, 5995–5999 https://doi.org/10.1073/pnas.1118355109
57. Fani L, Georgakis MK, Ikram MA, Ikram MK, Malik R, Dichgans M (2021) Circulating biomarkers of immunity and inflammation, risk of Alzheimer's disease, and hippocampal volume: a Mendelian randomization study. Transl Psychiatry 11:291. https://doi.org/10.1038/s41398-021-01400-z
58. Sapolsky RM, Krey LC, McEwen BS (1986) The neuroendocrinology of stress and aging: the glucocorticoid cascade hypothesis. Endocr Rev 7:284–301. https://doi.org/10.1210/edrv-7-3-284
59. Quattropani C, Vogt B, Odermatt A, Dick B, Frey BM, Frey FJ (2001) Reduced activity of 11beta-hydroxysteroid dehydrogenase in patients with cholestasis. J Clin Invest 108:1299–1305. https://doi.org/10.1172/JCI12745
60. Stauffer A, Rochat MK, Dick B, Frey FJ, Odermatt A (2002) Chenodeoxycholic acid and deoxycholic acid inhibit 11beta-hydroxysteroid dehydrogenase type 2 and cause cortisol-induced transcriptional activation of the mineralocorticoid receptor. J Biol Chem 277:26286–26292. https://doi.org/10.1074/jbc.M201556200
61. Solomon A, Kivipelto M, Wolozin B, Zhou J, Whitmer RA (2009) Midlife serum cholesterol and increased risk of Alzheimer's and vascular dementia three decades later. Dement Geriatr Cogn Disord 28:75–80. https://doi.org/10.1159/000231980
62. Mielke MM, Zandi PP, Sjogren M, Gustafson D, Ostling S, Steen B, Skoog I (2005) High total cholesterol levels in late life associated with a reduced risk of dementia. Neurology 64:1689–1695. https://doi.org/10.1212/01.WNL.0000161870.78572.A5

63. Lerner AJ, Arnold SE, Maxfield E, Koenig A, Toth ME, Fortin B et al (2022) CYP46A1 activation by low-dose efavirenz enhances brain cholesterol metabolism in subjects with early Alzheimer's disease. Alzheimers Res Ther 14:198. https://doi.org/10.1186/s13195-022-01151-z
64. Santos JX, Rasga C, Marques AR, Martiniano H, Asif M, Vilela J, Oliveira G, Sousa L, Nunes A, Vicente AM (2022) A role for gene-environment interactions in autism spectrum disorder is supported by variants in genes regulating the effects of exposure to xenobiotics. Front Neurosci 16:862315. https://doi.org/10.3389/fnins.2022.862315
65. Ritchie ME, Phipson B, Wu D, Hu Y, Law CW, Shi W (2015) Smyth, limma powers differential expression analyses for RNA-sequencing and microarray studies. Nucleic Acids Res 43:e47. https://doi.org/10.1093/nar/gkv007
66. Benjamini Y, Hochberg Y (1995) Controlling the false discovery rate: a practical and powerful approach to multiple testing. J R Stat Soc B 57:289–300. https://doi.org/10.1111/j.2517-6161.1995.tb02031.x

Figures

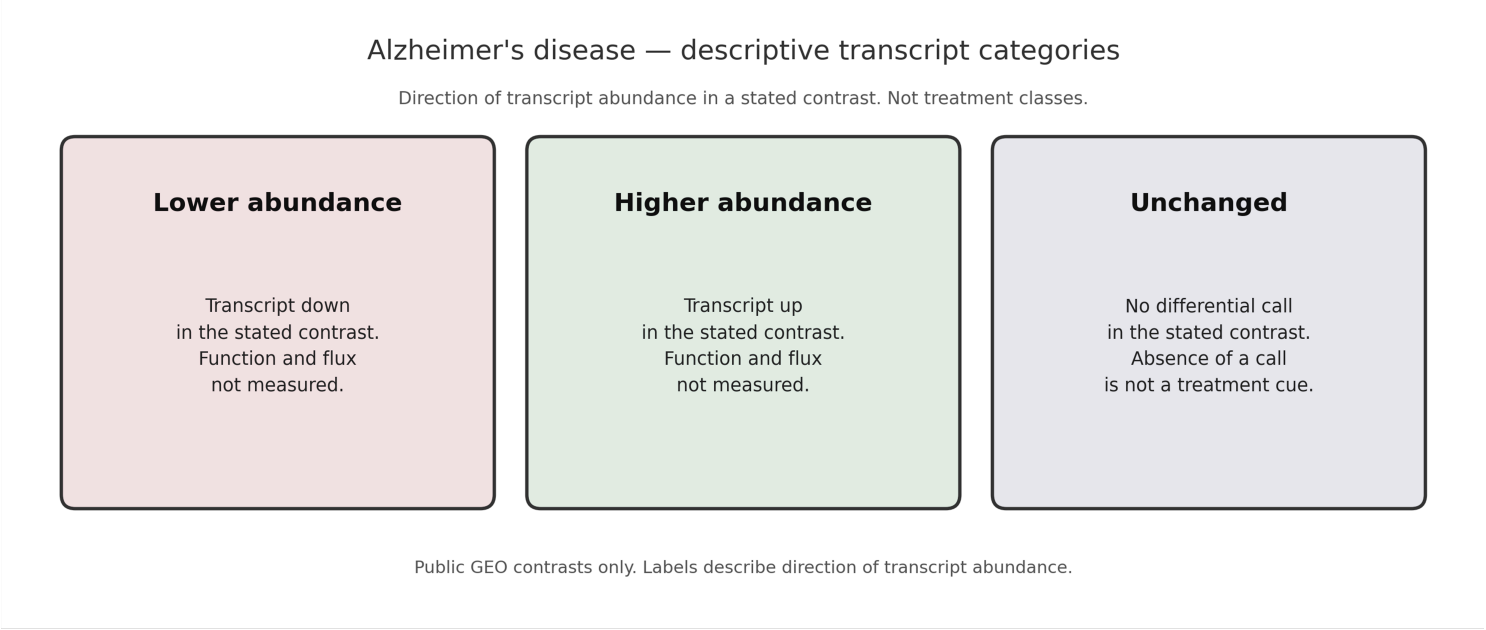


Figure 1

Descriptive transcript-direction categories in the AD contrasts. Boxes group panel genes by direction in a stated comparison: lower abundance, higher abundance, or unchanged abundance. A fourth grouping in the text is not a fourth direction but an annotation on one: genes whose observed direction carries a described biochemical consequence, such as higher EPHX2 in the L150P contrast. Direction is descriptive; the figure does not assign treatments, restoration targets, or pharmacological pushes.

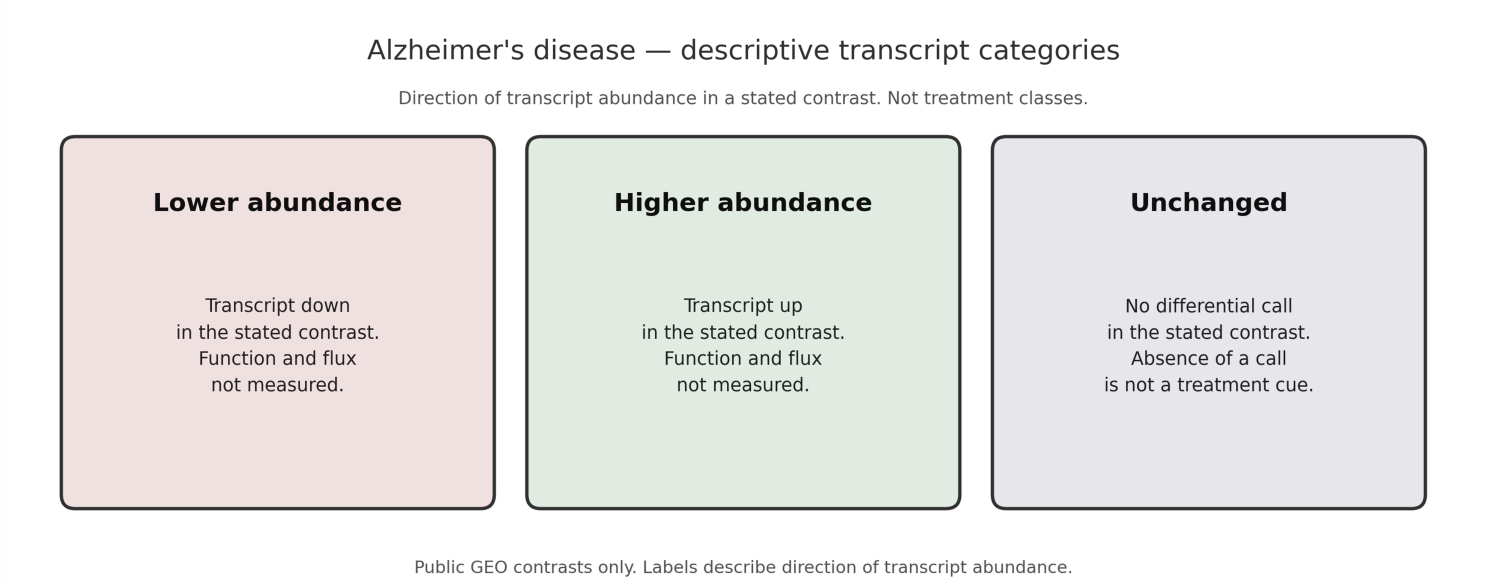


Figure 1

Descriptive transcript-direction categories in the AD contrasts. Boxes group panel genes by direction in a stated comparison: lower abundance, higher abundance, or unchanged abundance. A fourth grouping in the text is not a fourth direction but an annotation on one: genes whose observed direction carries a described biochemical consequence, such as higher EPHX2 in the L150P contrast. Direction is descriptive; the figure does not assign treatments, restoration targets, or pharmacological pushes.

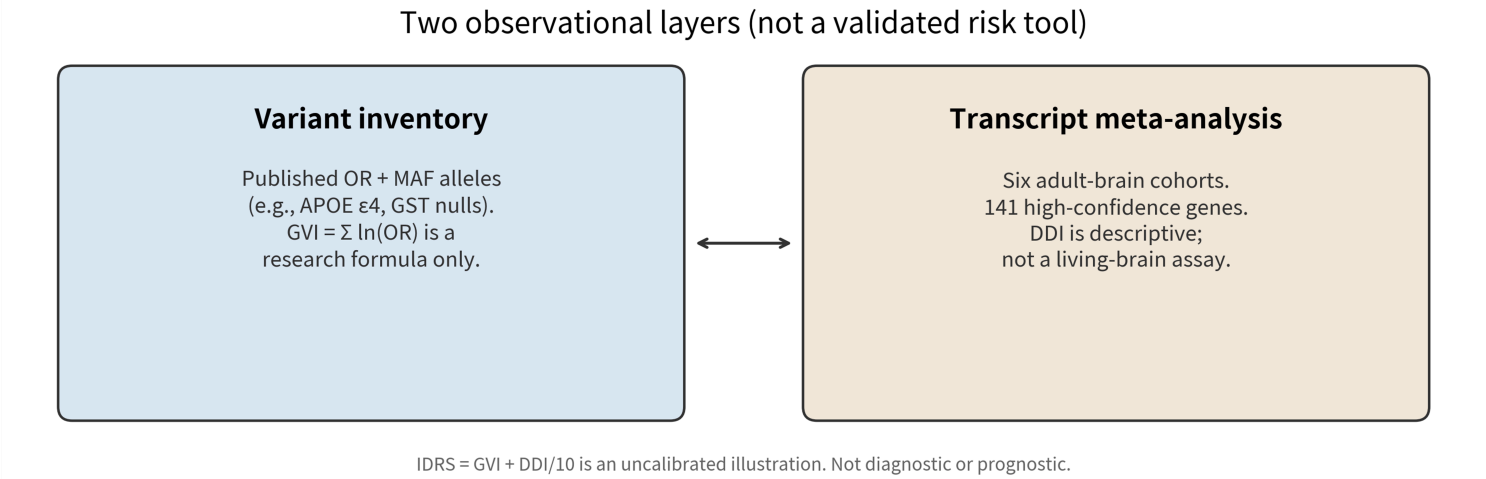


Figure 2

Variant inventory and transcript meta-analysis as parallel observational layers. GVI is a sum of published ln(OR) values used only in a simulation (n = 10,000; European-ancestry frequencies; median GVI 0.71). DDI is a descriptive per-dataset hit rate. IDRS = GVI + DDI/10 is an uncalibrated research formula, not a risk predictor. The two layers are not statistically combined into a clinical score.

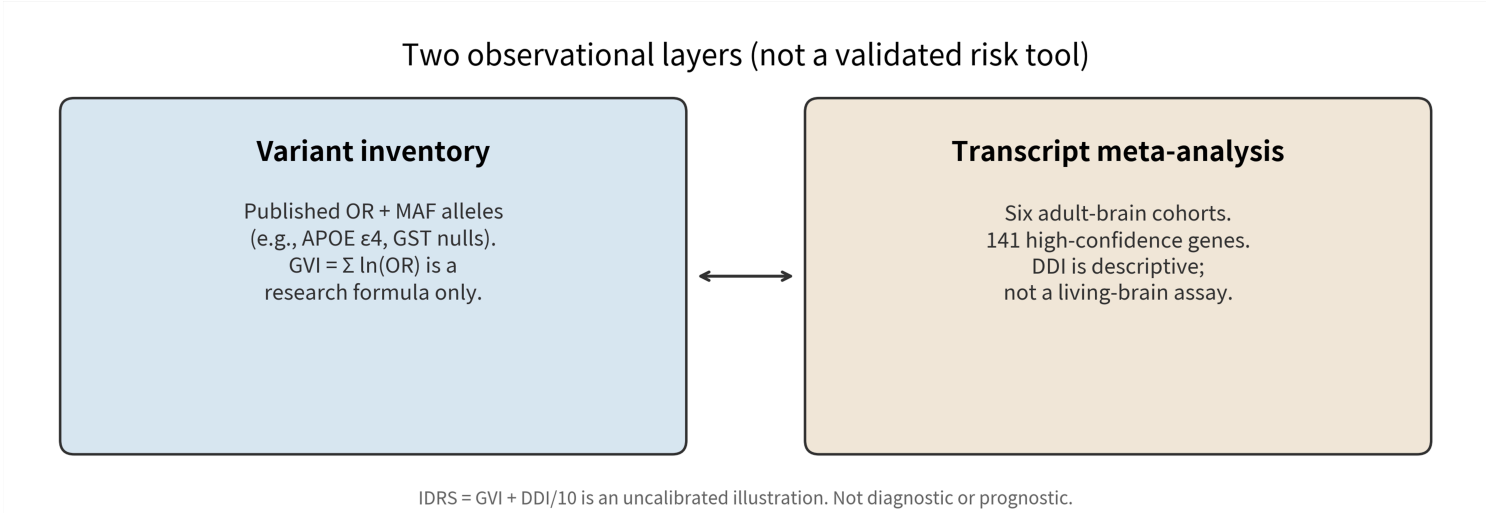


Figure 2

Variant inventory and transcript meta-analysis as parallel observational layers. GVI is a sum of published ln(OR) values used only in a simulation (n = 10,000; European-ancestry frequencies; median GVI 0.71). DDI is a descriptive per-dataset hit rate. IDRS = GVI + DDI/10 is an uncalibrated research formula, not a risk predictor. The two layers are not statistically combined into a clinical score.

Supplementary Files

This is a list of supplementary files associated with this preprint. Click to download.

- ADRSpackage20260910.zip
- ADRSpackage20260910.zip